

# Space is the Place: Effects of Continuous Spatial Structure on Analysis of Population Genetic Data

C.J. Battey<sup>\*,†</sup>, Peter L. Ralph<sup>\*,†</sup> and Andrew D. Kern<sup>\*,†</sup>

\*University of Oregon Dept. Biology, Institute for Ecology Evolution

**ABSTRACT** Real geography is continuous, but standard models in population genetics are based on discrete, well-mixed populations. As a result many methods of analyzing genetic data assume that samples are a random draw from a well-mixed population, but are applied to clustered samples from populations that are structured clinally over space. Here we use simulations of populations living in continuous geography to study the impacts of dispersal and sampling strategy on population genetic summary statistics, demographic inference, and genome-wide association studies. We find that most common summary statistics have distributions that differ substantially from that seen in well-mixed populations, especially when Wright's neighborhood size is less than 100 and sampling is spatially clustered. The combination of low dispersal and clustered sampling causes demographic inference from the site frequency spectrum to infer more turbulent demographic histories, but averaged results across multiple simulations were surprisingly robust to isolation by distance. We also show that the combination of spatially autocorrelated environments and limited dispersal causes genome-wide association studies to identify spurious signals of genetic association with purely environmentally determined phenotypes, and that this bias is only partially corrected by regressing out principal components of ancestry. Last, we discuss the relevance of our simulation results for inference from genetic variation in real organisms.

**KEYWORDS** Space; Population Structure; Demography; Haplotype block sharing; GWAS

25

## 26 **Introduction**

28 The inescapable reality that biological organisms live, move, and reproduce in continuous  
29 geography is usually omitted from population genetic models. However, mates tend to live  
30 near to one another and to their offspring, leading to a positive correlation between genetic

Manuscript compiled: Wednesday 15<sup>th</sup> May, 2019

<sup>1</sup>301 Pacific Hall, University of Oregon Dept. Biology, Institute for Ecology and Evolution. cbattey2@uoregon.edu.

<sup>†</sup>these authors co-supervised this project

31 differentiation and geographic distance. This pattern of “isolation by distance” (Wright 1943)  
32 is one of the most widely replicated empirical findings in population genetics (Aguillon *et al.*  
33 2017; Jay *et al.* 2012; Sharbel *et al.* 2000). Despite a long history of analytical work describing  
34 the genetics of populations distributed across continuous geography (e.g., Wright (1943);  
35 Rousset (1997); Barton *et al.* (2002, 2010); Ringbauer *et al.* (2017); Robledo-Arnuncio and  
36 Rousset (2010)), much modern work still describes geographic structure as a set of discrete  
37 populations connected by migration (e.g., Wright 1931; Epperson 2003; Rousset and Leblois  
38 2011; Shirk and Cushman 2014; Lundgren and Ralph 2018). For this reason, most population  
39 genetics statistics are interpreted with reference to discrete, well-mixed populations, and most  
40 empirical papers analyze variation within clusters of genetic variation inferred by programs  
41 like *STRUCTURE* (Pritchard *et al.* 2000) with methods that assume these are randomly mating  
42 units.

43 The assumption that populations are “well-mixed” has important implications for down-  
44 stream inference of selection and demography. Methods based on the coalescent (Kingman  
45 1982; Wakeley 2005) assume that the sampled individuals are a random draw from a well-  
46 mixed population that is much larger than the sample (Wakeley and Takahashi 2003). The  
47 key assumption is that the individuals of each generation are *exchangeable*, so that there is no  
48 correlation between the fate or fecundity of a parent and that of their offspring (Huillet and  
49 Möhle 2011). If dispersal or mate selection is limited by geographic proximity, this assump-  
50 tion can be violated in many ways. For instance, if mean viability or fecundity is spatially  
51 autocorrelated, then limited geographic dispersal will lead to parent–offspring correlations.  
52 Furthermore, nearby individuals will be more closely related than an average random pair, so  
53 drawing multiple samples from the same area of the landscape will represent a biased sample  
54 of the genetic variation present in the whole population (Städler *et al.* 2009).

55 Two areas in which spatial structure may be particularly important are demographic  
56 inference and genome-wide association studies (GWAS). Previous work has found that  
57 discrete population structure can create false signatures of population bottlenecks when  
58 attempting to infer demographic histories from microsatellite variation (Chikhi *et al.* 2010),  
59 statistics summarizing the site frequency spectrum (SFS) (Ptak and Przeworski 2002; Städler  
60 *et al.* 2009; St. Onge *et al.* 2012), or runs of homozygosity in a single individual (Mazet *et al.*  
61 2015). The increasing availability of whole-genome data has led to the development of many

62 methods that attempt to infer detailed trajectories of population sizes through time based on  
63 a variety of summaries of genetic data (Liu and Fu 2015; Schiffels and Durbin 2014; Sheehan  
64 *et al.* 2013; Terhorst *et al.* 2016). Because all of these methods assume that the populations being  
65 modeled are approximately randomly mating, they are likely affected by spatial biases in the  
66 genealogy of sampled individuals (Wakeley 1999), which may lead to incorrect inference of  
67 population changes over time (Mazet *et al.* 2015). However, previous investigations of these  
68 effects have focused on discrete rather than continuous space models, and the level of isolation  
69 by distance at which inference of population size trajectories become biased by structure is not  
70 well known. Here we test how two methods suitable for use with large samples of individuals  
71 – Stairwayplot (Liu and Fu 2015) and SMC++ (Terhorst *et al.* 2016) – perform when applied  
72 to populations evolving in continuous space with varying sampling strategies and levels of  
73 dispersal.

74 Spatial structure is also a major challenge for interpreting the results of genome-wide asso-  
75 ciation studies (GWAS). This is because many phenotypes of interest have strong geographic  
76 differences due to the (nongenetic) influence of environmental or socioeconomic factors,  
77 which can therefore show spurious correlations with spatially patterned allele frequencies  
78 (Bulik-Sullivan *et al.* 2015; Mathieson and McVean 2012). Indeed, two recent studies found  
79 that previous evidence of polygenic selection on human height in Europe was confounded  
80 by subtle population structure (Sohail *et al.* 2018; Berg *et al.* 2018), suggesting that existing  
81 methods to correct for population structure in GWAS are insufficient. However we have little  
82 quantitative idea of the population and environmental parameters that can be expected to  
83 lead to biases in GWAS.

84 Last, some of the most basic tools of population genetics are summary statistics like  $F_{IS}$  and  
85 Tajima's  $D$ , which are often interpreted as reflecting the influence of selection or demography  
86 on sampled populations (Tajima 1989). Statistics like Tajima's  $D$  are essentially summaries  
87 of the site frequency spectrum, which itself reflects variation in branch lengths and tree  
88 structure of the underlying genealogies of sampled individuals. Geographically limited mate  
89 choice distorts the distribution of these genealogies (Maruyama 1972; Wakeley 1999), which  
90 can affect the value of Tajima's  $D$  (Städler *et al.* 2009). Similarly, the distribution of tract  
91 lengths of identity by state among individuals contains information about not only historical  
92 demography (Harris and Nielsen 2013; Ralph and Coop 2013) and selection (Garud *et al.*

93 2015), but also dispersal and mate choice (Ringbauer *et al.* 2017; Baharian *et al.* 2016). We are  
94 particularly keen to examine how such summaries will be affected by models that incorporate  
95 continuous space, both to evaluate the assumptions underlying existing methods and to  
96 identify where the most promising signals of geography lie.

97 To study this, we have implemented an individual-based model in continuous geography  
98 that incorporates overlapping generations, local dispersal of offspring, and density-dependent  
99 survival. We simulate chromosome-scale genomic data in tens of thousands of individuals  
100 from parameter regimes relevant to common subjects of population genetic investigation such  
101 as humans and *Drosophila*, and output the full genealogy and recombination history of all  
102 final-generation individuals. We use these simulations to test how sampling strategy interacts  
103 with geographic population structure to cause systematic variation in population genetic  
104 summary statistics typically analyzed assuming discrete population models. We then examine  
105 how the fine-scale spatial structures occurring under limited dispersal impact demographic  
106 inference from the site frequency spectrum. Last, we examine the impacts of continuous  
107 geography on genome-wide association studies (GWAS) and identify regions of parameter  
108 space under which the results from GWAS may be misleading.

## 109 Materials and Methods

### 110 *Modeling Evolution in Continuous Space*

111 The degree to which genetic relationships are geographically correlated depends on the  
112 chance that two geographically nearby individuals are close relatives – in modern terms, by  
113 the tension between migration (the chance that one is descended from a distant location) and  
114 coalescence (the chance that they share a parent). A key early observation (by Wright 1943) is  
115 that this balance is nicely summarized by the “neighborhood size”, defined to be  $N_W = 4\pi\rho\sigma^2$ ,  
116 where  $\sigma$  is the mean parent–offspring distance and  $\rho$  is population density. This can be thought  
117 of as proportional to the average number of potential mates for an individual (those within  
118 distance  $2\sigma$ ), or the number of potential parents of a randomly chosen individual. Empirical  
119 estimates of neighborhood size vary hugely across species (see Discussion), but for reference  
120 estimates in human populations range from 40 to over 5,000 depending on the population  
121 and method of estimation (Table 1).

122 The first approach to modeling continuously-distributed populations was to endow indi-

123 viduals in a Wright-Fisher model with locations in continuous space. However, since the total  
124 size of the population is constrained, this introduces interactions between arbitrarily distant  
125 individuals, which (aside from being implausible) Felsenstein (1975) showed would eventually  
126 lead to unrealistic population clumping if the range is sufficiently large. Another method  
127 for modeling spatial populations is to assume the existence of a grid of discrete randomly-  
128 mating populations connected by migration, thus enforcing regular population density by  
129 edict. Among many other important results drawn from this class of “lattice” or “stepping  
130 stone” models, Rousset (1997) showed that the slope of the a linear regression of genetic  
131 differentiation ( $F_{ST}$ ) against the logarithm of spatial distance is an estimate of neighborhood  
132 size. Although these grid models are likely good approximations of continuous geography  
133 in many situations, they do not model demographic fluctuations, and limit investigation of  
134 spatial structure below the level of the deme, assumptions whose impacts are unknown. An  
135 alternative method for dealing with continuous geography is a new class of coalescent models,  
136 the Spatial Lambda Fleming-Viot models (Barton *et al.* 2010; Kelleher *et al.* 2014).

137 To avoid questionable assumptions, we here used forwards-time, individual-based sim-  
138 ulations. By scaling the probability of survival in each timestep to local population density  
139 we shift reproductive output towards low-density regions, which prevents populations from  
140 clustering. Such models have been used extensively in ecological modeling but rarely in  
141 population genetics, where to our knowledge previous implementations of continuous space  
142 models have focused on a small number of genetic loci, which limits the ability to investi-  
143 gate the impacts of continuous space on genome-wide genetic variation as is now routinely  
144 sampled from real organisms. By simulating chromosome-scale sequence alignments and  
145 complete population histories we are able to treat our simulations as real populations and  
146 replicate the sampling designs and analyses commonly conducted on real genomic data.

#### 147 **A Forward-Time Model of Evolution in Continuous Space**

148 We simulated populations using the non-Wright-Fisher module in the program SLiM v3.0  
149 (Haller and Messer 2019). Each time step consists of three stages: reproduction, dispersal, and  
150 mortality. To reduce the parameter space we use the same parameter, denoted  $\sigma$ , to modulate  
151 the spatial scale of interactions at all three stages by adjusting the standard deviation of the  
152 corresponding Gaussian functions. As in previous work (Wright 1943; Ringbauer *et al.* 2017),

153  $\sigma$  as applied in our dispersal step is equal to the mean parent-offspring distance.

154 At the beginning of the simulation individuals are distributed uniformly at random on  
155 a continuous, square landscape. Individuals are hermaphroditic, and each time step, each  
156 produces a Poisson number of offspring with mean  $1/L$  where  $L$  is the expected lifespan.  
157 Offspring disperse a Gaussian-distributed distance away from the parent with mean zero  
158 and standard deviation  $\sigma$  in both the  $x$  and  $y$  coordinates, reflected to stay within the species  
159 range. Each offspring is produced with a mate selected randomly from those within distance  
160  $3\sigma$ , with probability of choosing a neighbor at distance  $x$  proportional to  $\exp(-x^2/2\sigma^2)$ .

To maintain a stable population, mortality increases with local population density. To do this we say that individuals at distance  $d$  have a competitive interaction with strength  $g(d)$ , where  $g$  is the Gaussian density with mean zero and standard deviation  $\sigma$ . Then, the sum of all competitive interactions with individual  $i$  is  $n_i = \sum_j g(d_{ij})$ , where  $d_{ij}$  is the distance between individuals  $i$  and  $j$  and the sum is over all neighbors within distance  $3\sigma$ . Since  $g$  is a probability density,  $n_i$  is an estimate of the number of nearby individuals per unit area. Then, given a per-unit carrying capacity  $K$ , the probability of survival until the next time step for individual  $i$  is

$$p_i = \min \left( 0.95, \frac{1}{1 + n_i / (K(1 + L))} \right). \quad (1)$$

161 We chose this functional form so that the equilibrium population density per unit area is  
162 around  $K$ , and the mean lifetime is around  $L$ .

An important step in creating any spatial model is dealing with range edges. Because local population density is used to model competition, edge or corner populations can be assigned artificially high fitness values because they lack neighbors within their interaction radius but outside the bounds of the simulation. We approximate a decline in habitat suitability near edges by decreasing the probability of survival proportional to the square root of distance to edges in units of  $\sigma$ . The final probability of survival for individual  $i$  is then

$$s_i = p_i \min(1, \sqrt{x_i/\sigma}) \min(1, \sqrt{y_i/\sigma}) \min(1, \sqrt{(W - x_i)/\sigma}) \min(1, \sqrt{(W - y_i)/\sigma}) \quad (2)$$

163 where  $x_i$  and  $y_i$  are the spatial coordinates of individual  $i$ , and  $W$  is the width (and height) of  
164 the square habitat. This buffer roughly counteracts the increase in fitness individuals close to  
165 the edge would otherwise have.

166 To isolate spatial effects from other components of the model such as overlapping gener-

167 ations, increased variance in reproductive success, and density-dependent fitness, we also  
168 implemented simulations identical to those above except that mates are selected uniformly  
169 random from the population, and offspring disperse to a uniform random location on the  
170 landscape. We refer to this model as the “random mating” model, in contrast to the first,  
171 “spatial” model.

172 We stored the full genealogy and recombination history of final-generation individuals as  
173 tree sequences (Kelleher *et al.* 2018), as implemented in SLiM (Haller *et al.* 2019). Scripts for  
174 figures and analyses are available at <https://github.com/petrelharp/spaceness>.

175 We ran 400 simulations for the spatial and random-mating models on a square landscape  
176 of width  $W = 50$  with per-unit carrying capacity  $K = 5$  (census  $N \approx 10,000$ ), average lifetime  
177  $L = 4$ , genome size  $= 10^8$ , recombination rate  $= 10^{-9}$ , and drawing  $\sigma$  values from a uniform  
178 distribution between 0.2 and 4. To speed up the simulations and limit memory overhead  
179 we used a mutation rate of 0 in SLiM and later applied mutations to the tree sequence  
180 with msprime’s `mutate` function (Kelleher *et al.* 2016). Because msprime applies mutations  
181 proportionally to elapsed time, we divided the mutation rate of  $10^{-8}$  mutations per site per  
182 generation by the average generation time estimated for each value of  $\sigma$  (see ‘Demographic  
183 Parameters’ below) to convert the rate to units of mutations per site per unit time. (We verified  
184 that this procedure produced the correct number of mutations by comparing to a subset of  
185 simulations with SLiM-generated mutations, which are applied only at meiosis.) Simulations  
186 were run for 1.6 million timesteps (approximately  $30N$  generations).

### 187 **Demographic Parameters**

188 Our demographic model includes parameters for population density ( $K$ ), mean life span ( $L$ ),  
189 and dispersal distance ( $\sigma$ ). However, nonlinearity of local demographic stochasticity causes  
190 actual realized averages of these demographic quantities to deviate from the specified values  
191 in a way that depends on the neighborhood size. Therefore, to properly compare to theoretical  
192 expectations, we empirically calculated these demographic quantities in simulations. We  
193 recorded the census population size in all simulations. To estimate generation times, we stored  
194 ages of the parents of every new individual born across 200 timesteps, after a 100 generation  
195 burn-in, and took the mean. To estimate variance in offspring number, we tracked the number  
196 of offspring for all individuals for 100 timesteps following a 100-timestep burn-in period,

197 subset the resulting table to include only the last timestep recorded for each individual, and  
198 calculated the variance in number of offspring across all individuals in timesteps 50-100. All  
199 calculations were performed with information recorded in the tree sequence, using pslim  
200 (<https://github.com/tskit-dev/pyslim>).

201 **Sampling**

202 Our model records the genealogy and sequence variation of the complete population, but in  
203 real data, genotypes are only observed from a relatively small number of sampled individuals.  
204 We modeled three sampling strategies similar to common data collection methods in empirical  
205 genetic studies (Figure 1). “Random” sampling selects individuals at random from across  
206 the full landscape, “point” sampling selects individuals proportional to their distance from  
207 four equally spaced points on the landscape, and “midpoint” sampling selects individuals in  
208 proportion to their distance from the middle of the landscape. Downstream analyses were  
209 repeated across all sampling strategies.

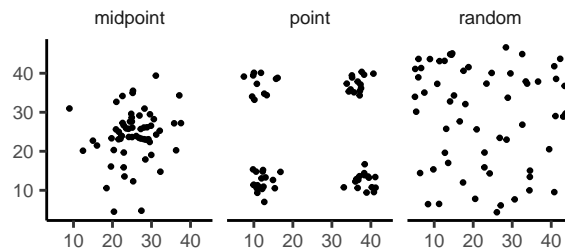


**Figure 1** Example sampling maps for 60 individuals on a  $50 \times 50$  landscape for midpoint, point, and random sampling strategies, respectively.

210 **Summary Statistics**

211 We calculated the site frequency spectrum and a set of 18 summary statistics (Table S1) from  
212 60 diploid individuals sampled from the final generation of each simulation using the python  
213 package scikit-allel (Miles and Harding 2017). Statistics included common single-population  
214 summaries including mean pairwise divergence ( $\pi$ ), inbreeding coefficient ( $F_{IS}$ ), and Tajima’s  
215  $D$ , as well as the classic isolation-by-distance regression of genetic distance ( $D_{xy}$ ) against the  
216 logarithm of geographic distances (Rousset 1997), which we summarized as the correlation  
217 coefficient between the logarithm of the spatial distance and the proportion of identical base  
218 pairs across pairs of individuals.

Following recent studies that showed strong signals for dispersal and demography in the distribution of shared haplotype block lengths (Ringbauer *et al.* 2017; Baharian *et al.* 2016), we also calculated various summaries of the distribution of pairwise identical-by-state (IBS) block lengths among samples. The full distribution of lengths of IBS tracts for each pair of chromosomes was first calculated with a custom python function. We then calculated the first three moments of this distribution (mean, variance, and skew) and the number of blocks over  $10^6$  base pairs both for each pair of individuals and for the full distribution across all pairwise comparisons.

We then estimated correlation coefficients between spatial distance and each moment of the pairwise IBS tract distribution. Because more closely related individuals on average share longer haplotype blocks we expect that spatial distance will be negatively correlated with mean haplotype block length, and that this correlation will be strongest (i.e., most negative) when dispersal is low. The variance, skew, and count of long haplotype block statistics are meant to reflect the relative length of the right (upper) tail of the distribution, which represents the frequency of long haplotype blocks, and so should reflect recent demographic events (Chapman and Thompson 2002). For a subset of simulations, we also calculated cumulative distributions for IBS tract lengths across pairs of distant ( $>48$  map units) and nearby ( $<2$  map units) individuals. Last, we examined the relationship between allele frequency and the spatial dispersion of an allele by calculating the average distance among individuals carrying each derived allele in a set of simulations representing a range of neighborhood sizes.

The effects of sampling on summary statistic estimates were summarized by testing for differences in mean (ANOVA, (R Core Team 2018)) and variance (Levene's test, (Fox and Weisberg 2011)) across sampling strategies for each summary statistic.

## Demographic Modeling

To assess the impacts of continuous spatial structure on demographic inference we inferred population size histories for all simulations using two approaches: Stairwayplot (Liu and Fu 2015) and SMC++ (Terhorst *et al.* 2016). Stairwayplot fits its model to a genome-wide estimate of the SFS, while SMC++ also incorporates information about linkage disequilibrium across the genome in a sequentially markovian coalescent framework. For both methods we sampled 20 individuals from all spatial simulations using random, midpoint, and point

249 sampling strategies.

250 Stairwayplot documentation suggests fitting models across multiple bootstrap replicates  
251 drawn from empirical genomic data and taking the median inferred  $N_e$  per unit time as the  
252 best estimate. We calculated site frequency spectra in scikit-allel (Miles and Harding 2017),  
253 generated 100 bootstrap replicates per simulation by resampling over sites, and fit models for  
254 all bootstrap samples using default settings in stairwayplot.

255 For SMC++ we first converted simulated genotype matrices to VCFs with msprime and  
256 then used SMC++’s standard pipeline for preparing input files assuming no polarization error  
257 in the SFS. We used the first individual in the VCF as the “designated individual” when fitting  
258 models, and allowed the program to estimate the recombination rate during optimization. We  
259 fit models using the ‘estimate’ command rather than the now recommended cross-validation  
260 approach because our simulations had only a single contig.

261 To evaluate the performance of these methods we binned simulations by neighborhood  
262 size, took a rolling median of inferred  $N_e$  trajectories across all model fits in a bin for each  
263 method and sampling strategy, and compared these values to the mean  $N_e$  of random-mating  
264 simulations estimated from  $\Theta_\pi$ . We also examined how varying levels of isolation by distance  
265 impacted the variance of  $N_e$  estimates by calculating the standard deviation of  $N_e$  from each  
266 best-fit model and plotting these against neighborhood size.

## 267 **Association Studies**

268 To assess the degree to which spatial structure confounds GWAS we simulated four types of  
269 nongenetic phenotype variation for 1000 randomly sampled individuals in each spatial SLiM  
270 simulation and conducted a linear regression GWAS with principal components as covariates  
271 in PLINK (Purcell *et al.* 2007). SNPs with a minor allele frequency less than 0.5% were excluded  
272 from this analysis. Phenotype values were set to vary by two standard deviations across  
273 the landscape in a rough approximation of the variation seen in height across Europe (*need*  
274 *citation*). Conceptually our approach is similar to that taken in Mathieson and McVean (2012),  
275 though here we model fully continuous spatial variation and compare GWAS output across a  
276 range of dispersal distances.

277 In all simulations, the phenotype of each individual is determined by adding independent  
278 Gaussian noise with mean zero and standard deviation 10 to a mean that may depend on

279 spatial position. We adjust the geographic pattern of mean phenotype to reflect spatially  
280 autocorrelated environmental influences on phenotype. In the first simulation of *nonspatial*  
281 environments, the mean did not change, so that all individuals' phenotypes were drawn  
282 independently from a Gaussian distribution with mean 110 and standard deviation 10. Next,  
283 to simulate *clinal* environmental influences on phenotype, we increased the mean phenotype  
284 from 100 on the left edge of the range to 120 on the right edge (two phenotypic standard  
285 deviations). Concretely, an individual at position  $(x, y)$  in a  $50 \times 50$  landscape has mean  
286 phenotype  $100 + 2x/5$ . Third, we simulated a more concentrated "corner" environmental  
287 effect by setting the mean phenotype for individuals with both  $x$  and  $y$  coordinates below 20  
288 to 120 (two standard deviations above the rest of the map). Finally, in "patchy" simulations we  
289 selected 10 random points on the map and set the mean phenotype of all individuals within  
290 three map units of each of these points to 120.

291 We performed principal components analysis (PCA) using scikit-allel (Miles and Harding  
292 2017) on the matrix of derived allele counts by individual for each simulation. SNPs were  
293 first filtered to remove strongly linked sites by calculating LD between all pairs of SNPs in  
294 a 200-SNP moving window and dropping one of each pair of sites with an  $R^2$  over 0.1. The  
295 LD-pruned allele count matrix was then centered and all sites scaled to unit variance when  
296 conducting the PCA, following recommendations in Patterson *et al.* (2006).

297 We ran linear-model GWAS both with and without the first 10 principal components as  
298 covariates in PLINK and summarized results across simulations by counting the number of  
299 SNPs with  $p$ -value below 0.05 after adjusting for an expected false positive rate of less than 5%  
300 (Benjamini and Yekutieli 2001). We also examined  $p$  values for systemic inflation by estimating  
301 the expected values from a uniform distribution (because no SNPs were used when generating  
302 phenotypes), plotting observed against expected values for all simulations, and summarizing  
303 across simulations by finding the mean  $\sigma$  value in each region of quantile-quantile space.  
304 Results from all analyses were summarized and plotted with the 'ggplot2' (Wickham 2016)  
305 and "cowplot" (Wilke 2019) packages in R (R Core Team 2018).

306    **Results**

307    **Demographic Parameters**

308    Adjusting the spatial dispersal and interaction distance,  $\sigma$ , has a surprisingly large effect on  
309    demographic quantities that are usually fixed in Wright-Fisher models – the generation time,  
310    census population size, and variance in offspring number. These are shown in Figure 2. This  
311    occurs because, even though the “population density” ( $K$ ) and “mean lifetime” ( $L$ ) parameters  
312    were the same in all simulations, the strength of stochastic effects depends strongly on  $\sigma$ .  
313    For instance, the population density near to individual  $i$  (denoted  $n_i$  above) is computed by  
314    averaging over roughly  $N_W = 4\pi K\sigma^2$  individuals, and so has standard deviation proportional  
315    to  $1/\sqrt{N_W}$  – it is more variable at lower densities. (Recall that  $N_W$  is Wright’s neighborhood  
316    size.) Since the probability of survival is a nonlinear function of  $n_i$ , actual equilibrium  
317    densities and lifetimes differ from  $K$  and  $L$ . This is the reason that we included *random mating*  
318    simulations – where mate choice and offspring dispersal are both nonspatial – since this  
319    should preserve the random fluctuations in local population density while destroying any  
320    spatial genetic structure. We verified that random mating models retained no geographic  
321    signal by showing that summary statistics did not differ significantly between sampling  
322    regimes (Table S2), unlike in spatial models (discussed below).

323    There are a few additional things to note about Figure 2. First, all three quantities are  
324    non-monotone with neighborhood size. Census size largely declines as neighborhood size  
325    increases for both the spatial and random mating models. However, for spatial models this  
326    decline only begins for neighborhood size  $\geq 10$ . By a neighborhood sizes larger than 100, the  
327    spatial and random mating models are indistinguishable from one another, a sign that our  
328    simulations are performing as expected. Census sizes range from  $\approx 14,000$  at low  $\sigma$  in the  
329    random mating model to  $\approx 10,000$  for both models when neighborhood sizes approach 1,000.

330    Generation time similarly shows complex behavior with respect to neighborhood sizes,  
331    and varies between 5.2 and 4.9 timesteps per generation across the parameter range explored.  
332    Under both the spatial and random mating models, generation time reaches a minimum at a  
333    neighborhood size of around 50. Interestingly, under the range of neighborhood sizes that we  
334    examined, generation times between the random mating and spatial models are never quite  
335    equivalent – presumably this would cease to be the case at neighborhood sizes higher than  
336    we simulated here.

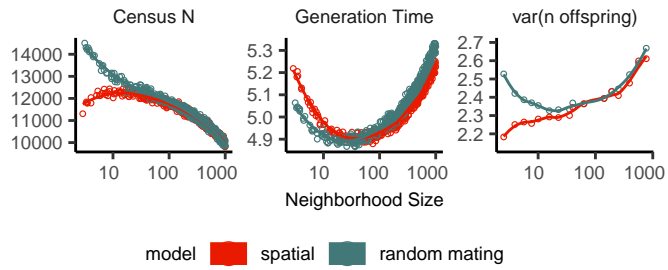


**Figure 2** Genealogical parameters from spatial and random mating SLiM simulations, by neighborhood size.

337 Last, we looked at the variance in number of offspring – a key parameter determining the  
 338 effective population size. Surprisingly, the spatial and random mating models behave quite  
 339 differently: while the variance in offspring number increases nearly monotonically under the  
 340 spatial model, the random mating model actually shows a decline in the variance in offspring  
 341 number until a neighborhood size  $\approx 10$  before it increases and eventually equals what we  
 342 observe in the spatial case.

343 **Impacts of Continuous Space on Population Genetic Summary Statistics**

344 Even though certain aspects of population demography depend on the scale of spatial inter-  
 345 actions, it still could be that population genetic variation is well-described by a well-mixed  
 346 population model. Indeed, mathematical results suggest that genetic variation in some spatial  
 347 models should be well-approximated by a Wright-Fisher population if neighborhood size is  
 348 large and all samples are geographically widely separated (Wilkins 2004; Zähle *et al.* 2005).  
 349 However, the behavior of most common population genetic summary statistics **other than**  
 350 **Tajima's D** (Städler *et al.* 2009) has not yet been described in realistic geographic models.  
 351 Moreover, as we will show, spatial sampling strategies can affect summaries of variation at  
 352 least as strongly as the underlying population dynamics.

353 **Site Frequency Spectra and Summaries of Diversity** Figure 3 shows the effect of varying  
 354 neighborhood size and sampling strategy on the site frequency spectrum (Figure 3A) and  
 355 several standard population genetic summary statistics (Figure 3B). **Consistent with findings**  
 356 **in n-island and stepping stone simulations** (Städler *et al.* 2009), the SFS shows a significant  
 357 enrichment of intermediate frequency variants in comparison to the nonspatial expectation.

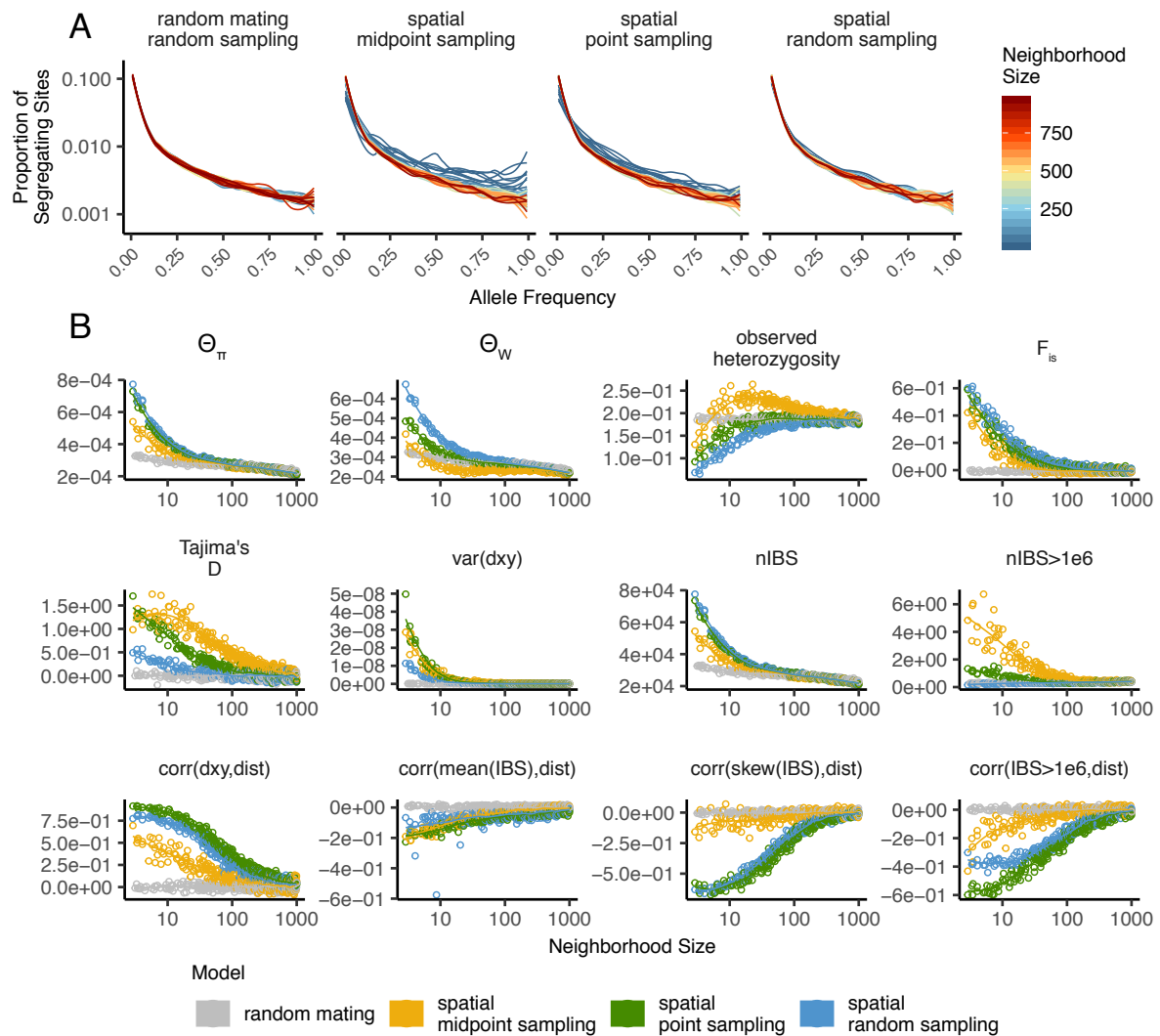


**Figure 3** Site frequency spectrum (A) and summary statistic distributions (B) by sampling strategy and neighborhood size.

358 This bias is most pronounced below neighborhood sizes  $\leq 100$  and is exacerbated by midpoint  
359 and point sampling of individuals (depicted in Figure 1). Reflecting this, Tajima's  $D$  is quite  
360 positive in the same situations (Figure 3B). Notably, the point at which Tajima's  $D$  approaches  
361 0 differs strongly across sampling strategies – varying from a neighborhood size of roughly 50  
362 for random sampling to at least 1000 for midpoint sampling.

363 One of the most commonly used summaries of variation is Tajima's summary of nucleotide  
364 divergence,  $\theta_\pi$ , calculated as the mean density of nucleotide differences averaged across pairs  
365 of samples. As can be seen in Figure 3B,  $\theta_\pi$  differs as much as nearly three-fold between the  
366 random mating and spatial models.  $\theta_\pi$  using each sampling strategy approaches the random  
367 mating expectation at its own rate, but by a neighborhood size of around 100 all models  
368 are equivalent. The differences between spatial and random mating simulations are much  
369 greater than expected from differences in census size divided by variance in offspring number.  
370 This likely occurs because  $\theta_\pi$  is a measure of mean time to most recent common ancestor  
371 between two samples, and at small values of  $\sigma$ , the time for dispersal to mix ancestry across  
372 the range exceeds the mean nonspatial coalescent time. (For instance, at the smallest value  
373 of  $\sigma = 0.2$ , the range is 250 dispersal distances wide, and since the location of a diffusively  
374 moving lineage after  $k$  generations has variance  $k\sigma^2$ , it takes around  $250^2 = 62500$  generations  
375 to mix across the range, which is roughly ten times larger than the random mating effective  
376 population size.) Interestingly, the effect of sampling strategy is reversed relative to that  
377 observed in Tajima's  $D$  – midpoint sampling reaches random mating expectations around  
378 neighborhood size 50, while random sampling is inflated until around neighborhood size 100.

379 Values of observed heterozygosity and its derivative  $F_{IS}$  also depend heavily on neighbor-  
380 hood size under spatial models as well as the sampling scheme.  $F_{IS}$  is inflated above the  
381 expectation across most of the parameter space examined and across all sampling strategies.  
382 This effect is caused by a deficit of heterozygous individuals in low-dispersal simulations  
383 – a continuous-space version of the Wahlund effect (Wahlund 1928). Indeed, for random  
384 sampling under the spatial model,  $F_{IS}$  does not approach the random mating equivalent until  
385 neighborhood sizes of nearly 1000. On the other hand, the dependency of raw observed  
386 heterozygosity on neighborhood size is not monotone. Under midpoint sampling observed  
387 heterozygosity is inflated even over the random mating expectation, as a result of the a higher  
388 proportion of heterozygotes occurring in the middle of the landscape (Figure S3). This squares

389 with a report from Shirk and Cushman (2014) who observed a similar excess of heterozygosity  
390 in the middle of the landscape when simulating under a lattice model.

391 **IBS tracts and correlations with geographic distance** We next turn our attention to the effect  
392 of geographic distance on haplotype block length sharing, summarized for sets of nearby and  
393 distant individuals in Figure 4. There are two main patterns to note. First, nearby individuals  
394 share more long IBS tracts than distant individuals (as expected because they are on average  
395 more closely related). Second, the difference in the number of long IBS tracts between nearby  
396 and distant individuals decreases as neighborhood size increases. This reflects the faster  
397 spatial mixing of populations with higher dispersal, which breaks down the correlation  
398 between the IBS tract length distribution and geographic distance. This can also be seen in the  
399 bottom row of Figure 3B, where the correlation coefficients between the summaries of the IBS  
400 tract length distribution (the mean, skew, and count of tracts over  $1 \times 10^6 bp$ ) and geographic  
401 distance approaches 0 as neighborhood size increases.

402 The patterns observed for correlations of IBS tract lengths with geographic distance are  
403 similar to those observed in the more familiar regression of allele frequency measures such as  
404  $D_{xy}$  (i.e. “genetic distance”) or  $F_{st}$  against geographic distance (Rousset 1997).  $D_{xy}$  is positively  
405 correlated with the geographic distance between the individuals, and the strength of this  
406 correlation declines as dispersal increases (Figure 3B), as expected under theory (Wright 1943;  
407 Rousset 1997). This relationship is very similar across random and point sampling strategies,  
408 but is weaker for midpoint sampling, perhaps due to a dearth of long-distance comparisons.  
409 In much of empirical population genetics a regression of genetic differentiation against spatial  
410 distance is a de-facto metric of the significance of isolation by distance. The similar behavior of  
411 moments of the pairwise distribution of IBS tract lengths shows why haplotype block sharing  
412 has recently emerged as a promising source of information on spatial demography through  
413 methods described in Ringbauer *et al.* (2017) and Baharian *et al.* (2016).

414 **Spatial distribution of allele copies** Mutations occur in individuals and spread geographically  
415 over time. Because low frequency alleles generally represent recent mutations (Sawyer 1977;  
416 Griffiths *et al.* 1999), the geographic dispersion of an allele may covary along with its frequency  
417 in the population. To visualize this relationship we calculated the average distance among  
418 individuals carrying a focal derived allele across simulations with varying neighborhood sizes,

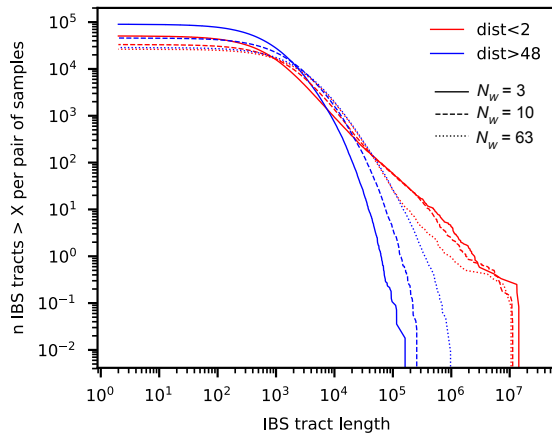


**Figure 4** Cumulative distributions for IBS tract lengths per pair of individuals at different geographic distances, across three neighborhood sizes ( $N_W$ ).

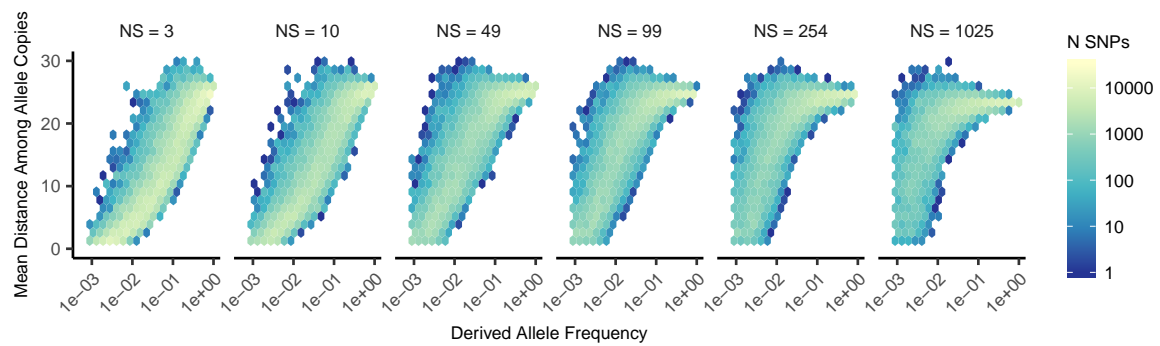


**Figure 5** Trends in the distance among allele copies at varying derived allele frequencies and neighborhood sizes.

419 shown in Figure 5. On average we find that low frequency alleles are the most geographically  
420 restricted, and that the extent to which geography and allele frequency are related depends on  
421 the amount of dispersal in the population. For populations with large neighborhood sizes we  
422 found that even very low frequency alleles can be found across the full landscape, whereas  
423 in populations with low neighborhood sizes the relationship between distance among allele  
424 copies and their frequency is quite strong. This is the basic process underlying Novembre and  
425 Slatkin (2009)'s method for estimating dispersal distances based on the distribution of low  
426 frequency alleles, and also generates the greater degree of bias in GWAS effect sizes for low  
427 frequency alleles identified in Mathieson and McVean (2012).

428 **Effects of Space on Demographic Inference**

429 One of the most important uses for population genetic data is inferring demographic history  
430 of populations. As demonstrated above, the site frequency spectrum and the distribution of  
431 IBS tracts varies across neighborhood sizes and sampling strategies. Does this variation lead to  
432 different inferences of past population sizes? To ask this we inferred population size histories  
433 from samples drawn from our simulated populations with two approaches: Stairwayplot  
434 (Liu and Fu 2015), which uses a genome-wide estimate of the SFS, and SMC++ (Terhorst *et al.*  
435 2016), which incorporates information on both the SFS and linkage disequilibrium across the  
436 genome.

437 Figure 6A shows the median inferred population size histories from each method, grouped  
438 by neighborhood size and sampling strategy. In general these methods tend to slightly overes-  
439 timate ancient population sizes and infer recent population declines when neighborhood sizes  
440 are below 20 and sampling is spatially clustered (Figure 6A, Figure S4). The overestimation of  
441 ancient population sizes however is relatively minor, averaging around a two-fold inflation  
442 at 10,000 generations before present in the worst-affected bins. For stairwayplot we found  
443 that many runs infer dramatic population bottlenecks in the last 1,000 generations when  
444 sampling is spatially concentrated, resulting in ten-fold or greater underestimates of recent  
445 population sizes. However SMC++ appeared more robust to this error, with runs on point-  
446 and midpoint-sampled simulations at the lowest neighborhood sizes underestimating recent  
447 population sizes by roughly half and those on randomly-sampled simulations showing little  
448 error. Above neighborhood sizes of around 100, both methods performed relatively well

449 when averaging across results from multiple simulations.

450 However, individual model fits from both methods frequently reflected turbulent demo-  
451 graphic histories (Figure S4), with the standard deviation of inferred  $N_e$  across time points  
452 often exceeding the expected  $N_e$  for both methods (Figure 6B). That is, despite the constant  
453 population sizes in our simulations, both methods tended to infer large fluctuations in popu-  
454 lation size over time, which could potentially result in incorrect biological interpretations. On  
455 average the variance of inferred population sizes was elevated at the lowest neighborhood  
456 sizes and declines as dispersal increases, with the strongest effects seen in stairwayplot model  
457 fits with for clustered sampling and neighborhood sizes less than 20 (Figure 6B).

#### 458 **GWAS**

459 To ask what confounding effects spatial genetic variation might have on genome-wide associa-  
460 tion studies we performed GWAS on our simulations using phenotypes that were determined  
461 solely by the environment – so, any SNP showing statistically significant correlation with  
462 phenotype is a false positive. As expected, spatial autocorrelation in the environment causes  
463 spurious associations across much of the genome if no correction for genetic relatedness  
464 among samples is performed (Figure 7, figure S5). This effect is particularly strong for clinal  
465 and corner environments, for which the lowest dispersal levels cause over 60% of SNPs in the  
466 sample to return significant associations. Patchy environmental distributions, which are less  
467 strongly spatially correlated (Figure 7A), cause fewer false positives overall but still produce  
468 spurious associations at roughly 10% of sites at the lowest neighborhood sizes. Interestingly  
469 we also observed a small number of false-positive associations in roughly 3% of analyses on  
470 simulations with nonspatial environments, both with and without PC covariates included in  
471 the regression.

472 The confounding effects of geographic structure are well known, and it is common practice  
473 to control for this by including principal components (PCs) as covariates to control for these  
474 effects. This mostly works in our simulations – after doing this, the vast majority of SNPs no  
475 longer surpass a 5% FDR significance threshold. However, a substantial number of SNPs – up  
476 to 1.5% at the lowest dispersal distances – still surpass this threshold (and thus would be false  
477 positives in a GWAS), especially under “corner” and “patchy” environmental distributions  
478 (Figure 7C). At neighborhood sizes larger than 500, up to 0.31% of SNPs were significant

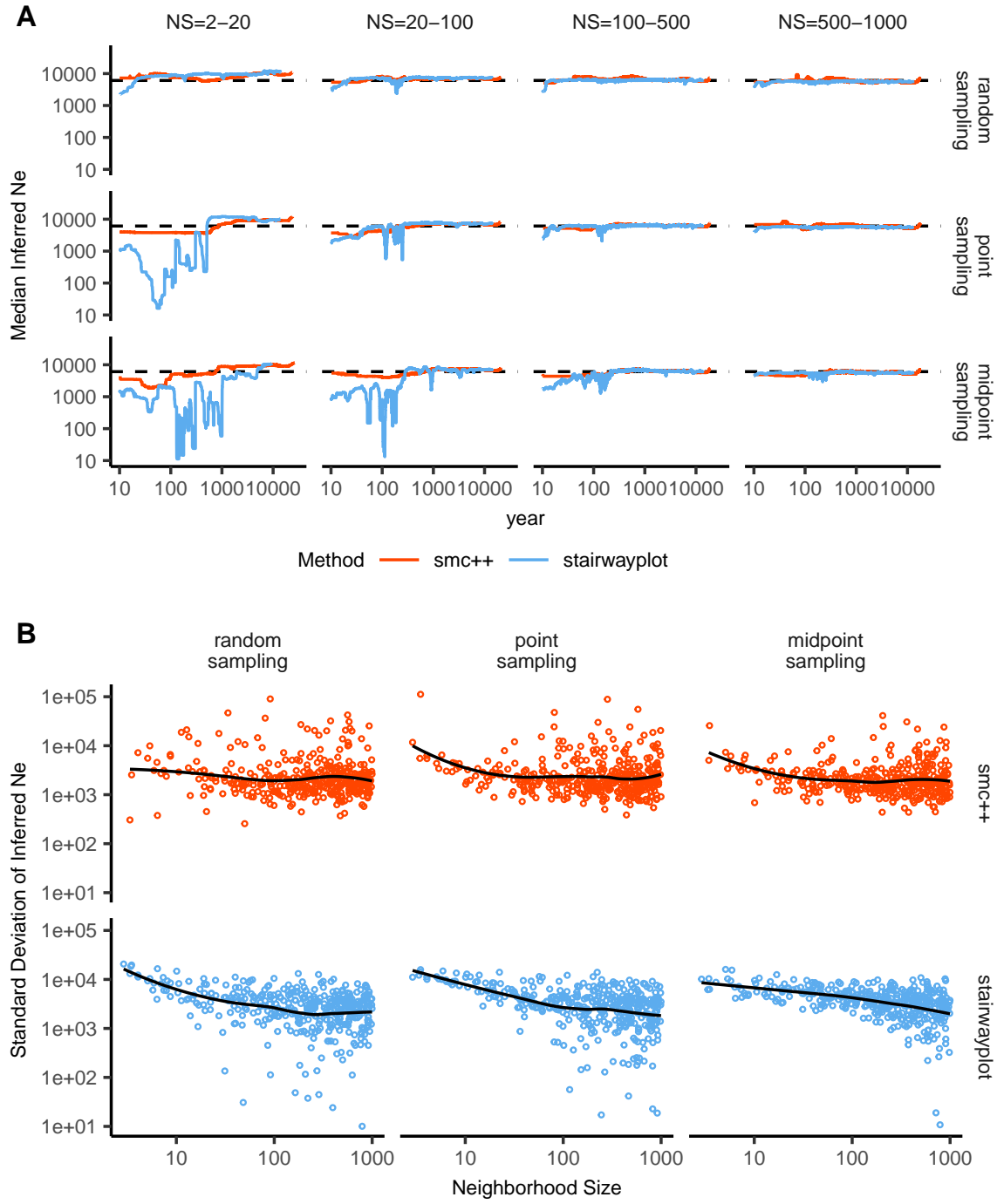


**Figure 6** A: Rolling median inferred  $N_e$  trajectories for `stairwayplot` and `smc++` across sampling strategies and neighborhood size bins. The dotted line shows the mean  $N_e$  of random-mating simulations. B: Standard deviation of individual inferred  $N_e$  trajectories, by neighborhood size and sampling strategy. Black lines are loess curves. Plots including individual model fits are shown in Figure S4.

479 for corner and clinal environments. Given an average of 132,000 SNPs across simulations  
480 after MAF filtering, this translates to up to 382 false-positive associations. In most cases the  
481  $p$  values for these associations were significant after FDR correction but would not pass the  
482 threshold for significance under the more conservative Bonferroni correction (see example  
483 manhattan plots in figure S5).

484 Clinal environments cause an interesting pattern in false positives after PC correction:  
485 at low neighborhood sizes the correction removes nearly all significant associations, but at  
486 neighborhood sizes above  $\approx 250$  the proportion of significant SNPs increases to up to 0.4%  
487 (Figure 7). This may be due to a loss of descriptive power of the PCs – as neighborhood size  
488 increases, the total proportion of variance explained by the first 10 PC axes declines from  
489 roughly 10% to 4% (Figure 7B). Essentially, PCA seems unable to effectively summarize the  
490 weak population structure present in large-neighborhood simulations, but these populations  
491 continue to have enough spatial structure to create significant correlations between genotypes  
492 and the environment. A similar process can also be seen in the corner phenotype distribution,  
493 in which the count of significant SNPs initially declines as neighborhood size increases and  
494 then increases at approximately the point at which the proportion of variance explained by  
495 PCA approaches its minimum.

496 Figure 7D shows quantile-quantile plots that show the degree of genome-wide inflation of  
497 test statistics in PC-corrected GWAS across all simulations and environmental distributions.  
498 For clinal environments,  $-\log_{10}(p)$  values are most inflated when neighborhood sizes are  
499 large, consistent with the pattern observed in the count of significant associations after  
500 PC regression. In contrast corner and patchy environments cause the greatest inflation  
501 in  $-\log_{10}(p)$  at neighborhood sizes  $< 100$ , which likely reflects the inability of PCA to  
502 account for fine-scale structure caused by very limited dispersal. Finally, we observed that PC  
503 regression appears to overfit to some degree for all phenotype distributions, visible in Figure  
504 7D as points falling below the 1:1 line.

## 505 Discussion

506 In this study, we have used efficient forward time population genetic simulations to describe  
507 the myriad influence of continuous geography on genetic variation. In particular, we examine  
508 how three main types of downstream empirical inference are affected by unmodeled spatial

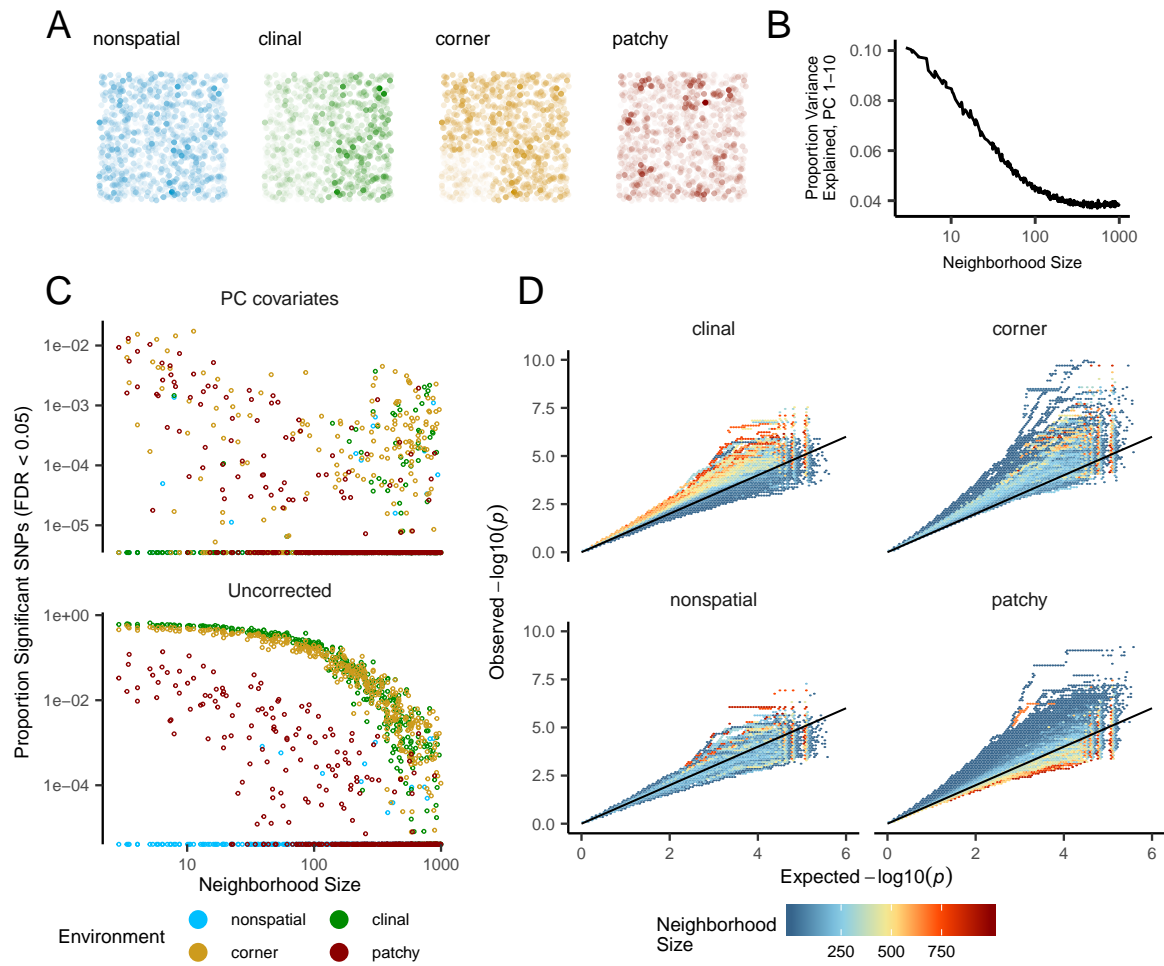


**Figure 7** Impacts of spatially varying environments and isolation by distance on linear regression GWAS. Simulated quantitative phenotypes are determined only by an individual's location and the spatial distribution of environmental factors. In **A** we show the phenotypes and locations of sampled individuals under four environmental distributions, with transparency scaled to phenotype. As neighborhood size increases a PCA explains less of the total variation in the data (**B**). Spatially correlated environmental factors cause false positives at a large proportion of SNPs, which is partially but not entirely corrected by adding PC positions as covariates (**C**). Quantile-quantile plots in **D** show inflation of  $-\log_{10}(p)$  after PC correction across all simulations and environmental distributions, with colors scaled by the median neighborhood size in each region of q-q space.

509 population structure – 1) population genetic summary statistics, 2) inference of population  
510 size history, and 3) genome-wide association studies (GWAS). As discussed above, space often  
511 matters (and sometimes dramatically), both because of how samples are arranged in space,  
512 and because of the inherent patterns of relatedness established by geography.

513 ***Effects of Dispersal***

514 Limited dispersal inflates effective population size, creates correlations between genetic and  
515 spatial distances, and introduces strong distortions in the site frequency spectrum that are  
516 reflected in a positive Tajima's  $D$  (Figure 3). At the lowest dispersal distances, this can increase  
517 genetic diversity threefold relative to random-mating expectations. These effects are strongest  
518 when neighborhood sizes are below 100, but in combination with the effects of nonrandom  
519 sampling they can persist up to neighborhood sizes of at least 1000 (e.g., inflation in Tajima's  
520  $D$  and observed heterozygosity under midpoint sampling). Under random sampling the  
521 general pattern is similar to expectations of the original analytic model of Wright (1943), which  
522 predicts that populations with neighborhood sizes under 100 will differ substantially from  
523 random mating, while those above 10,000 will be nearly indistinguishable from panmixia.

524 The patterns observed in sequence data reflect the effects of space on the underlying  
525 genealogy. Nearby individuals coalesce rapidly under limited dispersal and so are connected  
526 by short branch lengths, while distant individuals take much longer to coalesce than they  
527 would under random mating. Mutation and recombination events in our simulation both  
528 occur at a constant rate along branches of the genealogy, so the genetic distance and number  
529 of recombination events separating sampled individuals simply gives a noisy picture of the  
530 genealogies connecting them. Tip branches (i.e., branches subtending only one individual)  
531 are then relatively short, and branches in the middle of the genealogy connecting local groups  
532 of individuals relatively long, leading to the biases in the site frequency spectrum shown in  
533 Figure 3.

534 The genealogical patterns introduced by limited dispersal are particularly apparent in the  
535 distribution of haplotype block lengths (Figure 3). This is because identical-by-state tract  
536 lengths reflect the impacts of two processes acting along the branches of the underlying  
537 genealogy – both mutation and recombination – rather than just mutation as is the case  
538 when looking at the site frequency spectrum or related summaries. This means that the

539 pairwise distribution of haplotype block lengths carries with it important information about  
540 genealogical variation in the population, and correlation coefficients between moments of the  
541 this distribution and geographic location contain signal similar to the correlations between  
542  $F_{ST}$  or  $D_{xy}$  and geographic distance (Rousset 1997). Indeed this basic logic underlies two  
543 recent studies explicitly estimating dispersal from the distribution of shared haplotype block  
544 lengths (Ringbauer *et al.* 2017; Baharian *et al.* 2016). Conversely, because haplotype-based  
545 measures of demography are particularly sensitive to variation in the underlying genealogy,  
546 inference approaches that assume random mating when analyzing the distribution of shared  
547 haplotype block lengths are likely to be strongly affected by spatial processes.

548 **Effects of Sampling**

549 One of the most important differences between random mating and spatial models is the effect  
550 of sampling: in a randomly mating population the spatial distribution of sampling effort has  
551 no effect on estimates of genetic variation (Table S1), but when dispersal is limited sampling  
552 strategy can compound spatial patterns in the underlying genealogy and create pervasive  
553 impacts on all downstream genetic analyses (see also Städler *et al.* (2009)). In most species, the  
554 difficulty of traveling through all parts of a species range and the inefficiency of collecting  
555 single individuals at each sampling site means that most studies follow something closest  
556 to the “point” sampling strategy we simulated, in which multiple individuals are sampled  
557 from nearby points on the landscape. For example, in ornithology a sample of 10 individuals  
558 per species per locality is a common target when collecting for natural history museums. In  
559 classical studies of *Drosophila* variation the situation is considerably worse, in which a single  
560 orchard might be extensively sampled.

561 When sampling is clustered at points on a landscape and dispersal is limited, the sampled  
562 individuals will be more closely related than a random set of individuals. Average coalescence  
563 times of individuals collected at a locality will then be more recent and branch lengths shorter  
564 than expected by analyses assuming random mating. This leads to fewer mutations and  
565 recombination events occurring since their last common ancestor, causing a random set of  
566 individuals to share longer average IBS tracts and have fewer nucleotide differences. For some  
567 data summaries, such as Tajima’s  $D$ , Watterson’s  $\Theta$ , or the correlation coefficient between  
568 spatial distance and the count of long haplotype blocks, this can result in large differences in

569 estimates between random and point sampling (Figure 3). Inferring underlying demographic  
570 parameters from these summary statistics – unless the nature of the sampling is somehow  
571 taken into account – will be subject to bias if sampling is not random across the landscape.

572 However, the largest sampling effects we observed occurred in our “midpoint” sampling  
573 strategy. This model is meant to reflect a bias in sampling effort towards the middle of a species’  
574 range. In empirical studies this sampling strategy could arise if, for example, researchers  
575 choose to sample the center of the range and avoid range edges to maximize probability of  
576 locating individuals during a short field season. Because midpoint sampling provides limited  
577 spatial resolution it dramatically reduces the magnitude of observed correlations between  
578 spatial and genetic distances. More surprisingly, midpoint sampling also leads to strongly  
579 positive Tajima’s  $D$  and an inflation in the proportion of heterozygous individuals in the  
580 sample – similar to the effect of sampling a single deme in an n-island model as reported in  
581 (Städler *et al.* 2009). This increase in observed heterozygosity appears to reflect the effects of  
582 range edges, which are a fundamental facet of spatial genetic variation. If individuals move  
583 randomly in a finite two-dimensional landscape then regions in the middle of the landscape  
584 receive migrants from all directions while those on the edge receive no migrants from at least  
585 one direction. The average number of new mutations moving into the middle of the landscape  
586 is then higher than the number moving into regions near the range edge, leading to higher  
587 heterozygosity and lower inbreeding coefficients ( $F_{IS}$ ) away from range edges. Though here  
588 we used only a single parameterization of fitness decline at range edges we believe this is a  
589 general property of non-infinite landscapes as it has also been observed in previous studies  
590 simulating under lattice models (Neel *et al.* 2013; Shirk and Cushman 2014).

591 In summary, empirical researchers should collect individuals from across as much of the  
592 species’ range as practical, choosing samples at a variety of spatial scales. Many summary  
593 statistics are designed for well-mixed populations, and so provide different insights into  
594 genetic variation when applied to different subsets of the population. Applied to a cluster  
595 of samples, summary statistics based on segregating sites (e.g., Watterson’s  $\Theta$  and Tajima’s  
596  $D$ ), heterozygosity, or the distribution of long haplotype blocks, can be expected to depart  
597 significantly from what would be obtained from a wider distribution of samples. Comparing  
598 the results of analyses conducted on all individuals versus those limited to single individuals  
599 per locality can provide an informative contrast. Finally we wish to point out that the bias

600 towards intermediate allele frequencies that we observe may mean that the importance of  
601 linked selection, at least as is gleaned from the site frequency spectrum, may be systematically  
602 underestimated currently.

603 **Demography**

604 Previous studies have found that population structure and nonrandom sampling can create  
605 spurious signals of population bottlenecks when attempting to infer demographic history  
606 with microsatellite variation, summary statistics, or runs of homozygosity (Chikhi *et al.* 2010;  
607 Städler *et al.* 2009; Ptak and Przeworski 2002; Mazet *et al.* 2015). Here we found that methods  
608 that infer detailed population trajectories through time based on the SFS and patterns of LD  
609 across the genome are also subject to this bias, with some combinations of dispersal and  
610 sampling strategy inferring deep recent population bottlenecks and overestimating ancient  
611  $N_e$  by a around a factor of 2. However we were surprised to see that both Stairwayplot and  
612 SMC++ can tolerate relatively strong isolation by distance – i.e. neighborhood sizes of 20  
613 – and still perform well when averaging results across multiple simulations. Inference in  
614 populations with neighborhood sizes over 20 was relatively accurate unless samples were  
615 concentrated in the middle of the range (Figure 6). As we will discuss below, most empirical  
616 estimates of neighborhood size, including all estimates for human populations, are large  
617 enough that population size trajectories inferred by these approaches should not be strongly  
618 affected by spatial biases created by dispersal in continuous landscapes. In contrast, Mazet  
619 *et al.* (2015) found that varying migration rates through time could create strong biases in  
620 inferred population trajectories from an  $n$ -island model with parameters relevant for human  
621 history, suggesting that changes in migration rates through time are more likely to drive  
622 variation in inferred  $N_e$  than isolation by distance.

623 Between the two methods we tested, we found that SMC++ was more robust to spatial  
624 biases than Stairwayplot, with the worst-affected bins underestimating recent populations by  
625 roughly half rather than nearly 10-fold as with Stairwayplot. Though this degree of variation  
626 in population size is certainly meaningful in an ecological context, it is relatively minor in  
627 population genetic terms. A more worrying pattern was the high level of variance in inferred  
628  $N_e$  trajectories for individual model fits using these methods, which was highest in simulations  
629 with the smallest neighborhood size (Figure 6, Figure S4). This suggests that, at a minimum,

630 researchers working with empirical data should replicate analyses multiple times and take  
631 a rolling average if model fits are inconsistent across runs. Splitting samples and running  
632 replicates on separate subsets – the closest an empirical study can come to our design of  
633 averaging the results from multiple simulations – may also alleviate this issue.

634 In general however, our analysis suggests that many empirical analyses of population size  
635 history using methods like SMC++ are robust to error caused by spatial structure within  
636 continuous landscapes. Inferences drawn from static SFS-based methods like Stairwayplot  
637 should be treated with caution when there are signs of isolation by distance in the underlying  
638 data (for example, if a regression of  $F_{st}$  against the logarithm of geographic distance has a  
639 significantly positive slope), and in particular an inference of population bottlenecks in the last  
640 1000 years should be discounted if sampling is clustered, but estimates of deeper time patterns  
641 are likely to be fairly accurate. The biases in the SFS and haplotype structure identified above  
642 (see also (Wakeley 1999; Chikhi *et al.* 2010; Städler *et al.* 2009)) are apparently small enough  
643 that they fall within the range of variability regularly inferred by these approaches, at least on  
644 datasets of the size we simulated.

#### 645 **GWAS**

646 Spatial structure is particularly challenging for genome-wide association studies, because  
647 the effects of dispersal on genetic variation are compounded by spatial variation in the  
648 environment (Mathieson and McVean 2012). Spatially restricted mate choice and dispersal  
649 causes variation in allele frequencies across the range of a species. If environmental factors  
650 affecting the phenotype of interest also vary over space, then groups of individuals in different  
651 regions will both experience different environments and have different allele frequencies at  
652 many sites in the genome. In this scenario an uncorrected GWAS will infer genetic associations  
653 with a purely environmental phenotype at any site in the genome that is differentiated over  
654 space, and the relative degree of bias will be a function of the degree of covariation in allele  
655 frequencies and the environment (i.e. Figure 7C, bottom panel). This pattern is now well  
656 known and has been demonstrated in a variety of simulation and empirical contexts (Price  
657 *et al.* 2006; Yu *et al.* 2005; Young *et al.* 2018; Mathieson and McVean 2012; Kang *et al.* 2008, 2010;  
658 Bulik-Sullivan *et al.* 2015; Berg *et al.* 2018; Sohail *et al.* 2018).

659 Incorporating PC positions as covariates in a linear-regression GWAS (Price *et al.* 2006) is

660 designed to address this challenge by regressing out a baseline level of “average” differentiation.  
661 In essence, a PC-corrected GWAS asks “what regions of the genome are more associated  
662 with this phenotype than the average genome-wide association observed across populations?”  
663 In our simulations, we observed that this procedure can fail under a variety of circumstances.  
664 If dispersal is limited and environmental variation is clustered in space (i.e., corner or patchy  
665 distributions in our simulations), PCA positions fail to capture the fine-scale spatial structure  
666 required to remove all signals of association. Conversely, as dispersal increases, PCA loses  
667 power to describe population structure before spatial mixing breaks down the relationship  
668 between genotype and the environment. These effects were observed with all spatially cor-  
669 related environmental patterns, but were particularly pronounced if environmental effects  
670 are concentrated in one region, as was also found by Mathieson and McVean (2012). Though  
671 increasing the number of PC axes used in the analysis may reduce the false-positive rate, this  
672 may also decrease the power of the test to detect truly causal alleles (Lawson *et al.* 2019).

673 Here we simulated a single chromosome with size roughly comparable to one human  
674 chromosome. If we scale the number of false-positive associations identified in our anal-  
675 yses to a GWAS conducted on whole-genome data from humans, we would expect to see  
676 several thousand weak false-positive associations after PC corrections in a population with  
677 neighborhood sizes up to at least 1000 (which should include values appropriate for many  
678 human populations). Notably, very few of the spurious associations we identified would be  
679 significant at a conservative Bonferroni-adjusted *p*-value cutoff (see Figure S5). This suggests  
680 that GWAS focused on finding strongly associated alleles for traits controlled by a limited  
681 number of variants in the genome are likely robust to the impacts of continuous spatial struc-  
682 ture. However, methods that analyze the combined effects of thousands or millions of weakly  
683 associated variants such as polygenic risk scores (Khera *et al.* 2018) are likely to be affected by  
684 subtle population structure. Indeed as recently identified in studies of genotype associations  
685 for human height in Europe (Berg *et al.* 2018; Sohail *et al.* 2018), PC regression GWAS in  
686 modern human populations do include residual signal of population structure in large-scale  
687 analyses of polygenic traits. When attempting to make predictions across populations with  
688 different environmental exposures, PRS affected by population structure can be expected to  
689 offer low predictive power, as was shown in a recent study finding lower performance of PRS  
690 outside European populations (Martin *et al.* 2019).

691 In summary, spatial covariation in population structure and the environment confound the  
692 interpretation of GWAS *p*-values, and correction using principal components is insufficient to  
693 fully separate these signals for polygenic traits under a variety of environmental and popu-  
694 lation parameter regimes. Other GWAS methods may be less sensitive to this confounding,  
695 but there is no obvious reason that this should be so. One approach to estimating the degree  
696 of bias in GWAS caused by population structure is LD score regression (Bulik-Sullivan *et al.*  
697 2015). Though this approach appears to work well in practice, its interpretation is not always  
698 straightforward and it is likely biased by the presence of linked selection (Berg *et al.* 2018). **In**  
699 **addition, we observed that in many cases the false-positive SNPs we identified appeared to be**  
700 **concentrated in LD peaks similar to those expected from truly causal sites (Figure S5), which**  
701 **may confound LD score regression.** We suggest a straightforward alternative for species in  
702 which the primary axes of population differentiation is space (note this is likely not the case  
703 for some modern human populations): run a GWAS with spatial coordinates as phenotypes  
704 and check for *p*-value inflation or significant associations. If significant associations with  
705 sample locality are observed after correcting for population structure, the method is sensitive  
706 to false positives induced by spatial structure. This is essentially the approach taken in our  
707 “clinal” model (though we add normally distributed noise to our phenotypes). Of course, it is  
708 possible that genotypes indirectly affect individual locations by adjusting organismal fitness  
709 and thus habitat selection across spatially varying environments, but we believe that this  
710 hypothesis should be tested against a null of stratification bias inflation rather than accepted  
711 as true based on GWAS results.

712 **Where are natural populations on this spectrum?**

713 For how much of the tree of life do spatial patterns circumscribe genomic variation? In Table  
714 1 we gathered estimates of neighborhood size from a range of organisms to get an idea of  
715 how likely dispersal is to play an important role in patterns of variation. Though this sample  
716 is almost certainly biased towards small-neighborhood species (because few studies have  
717 quantified neighborhood size in species with very high dispersal or population density), we  
718 find that neighborhood sizes in the range we simulated are fairly common across a range of  
719 taxa. At the extreme low end of empirical neighborhood size estimates we see some flowering  
720 plants, large mammals, and colonial insects like ants. Species such as this have neighborhood

**Table 1 Neighborhood size estimates from empirical studies.**

Species	Description	Neighborhood Size	Method	Citation
<i>Ipomopsis aggregata</i>	flowering plant	12.60 - 37.80	Genetic	(Campbell and Dooley 1992)
<i>Borreria frutescens</i>	salt marsh plant	20 - 30	Genetic+Survey	(Antlfinger 1982)
<i>Oreamnos americanus</i>	mountain goat	36 - 100	Genetic	(Shirk and Cushman 2014)
<i>Homo sapiens</i>	Gainj- and Kalam-speaking people, Papua New Guinea	40 - 213	Genetic	(Rousset 1997)
<i>Formica sp.</i>	colonial ants	50 - 100	Genetic	(Pamilo 1983)
<i>Astrocaryum mexicanum</i>	palm tree	102 - 895	Genetic+survey	(Eguiarte <i>et al.</i> 1993)
<i>Spermophilus mollis</i>	ground squirrel	204 - 480	Genetic+Survey	(Antolin <i>et al.</i> 2001)
<i>Sceloporus olivaceus</i>	lizard	225 - 270	Survey	(Kerster 1964)
<i>Dieffenbachia longispatha</i>	beetle-pollinated colonial herb	227 - 611	Survey	(Young 1988)
<i>Homo sapiens</i>	Gainj- and Kalam-speaking people, Papua New Guinea	410	Survey	(Rousset 1997)
<i>Quercus laevis</i>	Oak tree	> 440	Genetic	(Berg and Hamrick 1995)
<i>Drosophila pseudoobscura</i>	fruit fly	500 - 1,000	Survey+Crosses	(Wright 1946)
<i>Homo sapiens</i>	POPRES data NE Europe	1,342 - 5,425	Genetic	(Ringbauer <i>et al.</i> 2017)
<i>Bebicium vittatum</i>	intertidal snail	240,000	Survey	(Rousset 1997)
<i>Bebicium vittatum</i>	intertidal snail	360,000	Genetic	(Rousset 1997)

size estimates small enough that spatial processes are likely to strongly influence inference. These include some human populations such as the Gainj- and Kalam-speaking people of Papua New Guinea, in which the estimated neighborhood sizes in (Rousset 1997) range from 40 to 410 depending on the method of estimation. Many more species occur in a middle range of neighborhood sizes between 100 and 1000 – a range in which spatial processes play a minor role in our analyses under random spatial sampling but are important when sampling of individuals in space is clustered. Last, many species likely have neighborhood sizes much larger than we simulated, including modern humans in NE Europe (Ringbauer *et al.* 2017). For these species demographic inference and summary statistics are likely to reflect minimal bias from spatial effects as long as dispersal is truly continuous across the landscape. While that is so we caution that association studies in which the effects of population structure are confounded with spatial variation in the environment are still sensitive to dispersal even at these large neighborhood sizes.

#### 734 ***Future Directions and Limitations***

As we have shown, a large number of population genetic summary statistics contain information about spatial population processes. We imagine that combinations of such summaries might be sufficient for the construction of supervised machine learning regressors (e.g., Schrider and Kern (2018)) for the accurate estimation of dispersal from genetic data. Indeed, Ashander *et al.* (2018) found that inverse interpolation on a vector of summary statistics provided a powerful method of estimating dispersal distances. Expanding this approach to include the haplotype-based summary statistics studied here and applying machine learning regressors built for general inference of nonlinear relationships from high-dimensional data may allow precise estimation of spatial parameters under a range of complex models.

One facet of spatial variation that we did not address in this study is the confounding of dispersal and population density implicit in the definition of Wright's Neighborhood Size. Our simulations were run under constant densities, but Ringbauer *et al.* (2017)'s approach to demographic inference in space suggests that density and dispersal can in some cases be estimated separately from genetic data. Much additional work remains to be done to better understand how these parameters interact to shape genetic variation in continuous space, which we leave to future studies.

Though our simulation allows incorporation of realistic demographic and spatial processes, it is inevitably limited by the computational burden of tracking tens or hundreds of thousands of individuals in every generation. In particular, computations required for mate selection and spatial competition scale approximately with the product of the total census size and the neighborhood size and so increases rapidly for large populations and dispersal distances. The reverse-time model of continuous space evolution described by Barton *et al.* (2010) and implemented by Kelleher *et al.* (2014) allows exploration of parameter regimes with population and landscape sizes more directly comparable to empirical cases like humans. Alternatively, implementation of parallelized calculations may allow progress with forwards-time simulations.

(removed section on recapitulation here)

Finally, we believe that the difficulties in correcting for population structure in continuous populations using principal components analysis or similar decompositions is a difficult issue, well worth considering on its own. How can we best avoid spurious correlations while correlating genetic and phenotypic variation without underpowering the methods? Perhaps optimistically, we posit that process-driven descriptions of ancestry and/or more generalized unsupervised methods may be able to better account for carry out this task.

## 768 Data Availability

769 Scripts used for all analyses and figures are available at <https://github.com/petrelharp/spaceness>.

## 770 Acknowledgements

771 We thank Brandon Cooper, and others for reading and thinking about this manuscript. We  
772 thank the Hearth for having such good, nearby coffee. Falling Sky Brewing was key to the  
773 success of this research endeavor. CJB and ADK were supported by NIH award R01GM117241.

## 774 Literature Cited

775 Aguillon, S. M., J. W. Fitzpatrick, R. Bowman, S. J. Schoech, A. G. Clark, *et al.*, 2017 Deconstruct-  
776 ing isolation-by-distance: The genomic consequences of limited dispersal. PLOS Genetics  
777 13: 1–27.

- 778 Antlfinger, A. E., 1982 Genetic neighborhood structure of the salt marsh composite, *Borrichia*  
779 *frutescens*. *Journal of Heredity* **73**: 128–132.
- 780 Antolin, M. F., B. V. Horne, M. D. Berger, Jr., A. K. Holloway, J. L. Roach, *et al.*, 2001 Effective  
781 population size and genetic structure of a piute ground squirrel (*Spermophilus mollis*)  
782 population. *Canadian Journal of Zoology* **79**: 26–34.
- 783 Ashander, J., P. Ralph, E. McCartney-Melstad, and H. B. Shaffer, 2018 Demographic inference  
784 in a spatially-explicit ecological model from genomic data: a proof of concept for the mojave  
785 desert tortoise. *bioRxiv* .
- 786 Baharian, S., M. Barakatt, C. R. Gignoux, S. Shringarpure, J. Errington, *et al.*, 2016 The great  
787 migration and african-american genomic diversity. *PLOS Genetics* **12**: 1–27.
- 788 Barton, N. H., F. Depaulis, and A. M. Etheridge, 2002 Neutral evolution in spatially continuous  
789 populations. *Theoretical Population Biology* **61**: 31–48.
- 790 Barton, N. H., J. Kelleher, and A. M. Etheridge, 2010 A new model for extinction and recolo-  
791 nization in two dimensions: Quantifying phylogeography. *Evolution* **64**: 2701–2715.
- 792 Benjamini, Y. and D. Yekutieli, 2001 The control of the false discovery rate in multiple testing  
793 under dependency. *The Annals of Statistics* **29**: 1165–1188.
- 794 Berg, E. E. and J. L. Hamrick, 1995 Fine-scale genetic structure of a turkey oak forest. *Evolution*  
795 **49**: 110–120.
- 796 Berg, J. J., A. Harpak, N. Sinnott-Armstrong, A. M. Joergensen, H. Mostafavi, *et al.*, 2018  
797 Reduced signal for polygenic adaptation of height in uk biobank. *bioRxiv* .
- 798 Bulik-Sullivan, B. K., P.-R. Loh, H. K. Finucane, S. Ripke, J. Yang, *et al.*, 2015 Ld score regression  
799 distinguishes confounding from polygenicity in genome-wide association studies. *Nature*  
800 *Genetics* **47**: 291 EP –.
- 801 Campbell, D. R. and J. L. Dooley, 1992 The spatial scale of genetic differentiation in a  
802 hummingbird-pollinated plant: Comparison with models of isolation by distance. *The*  
803 *American Naturalist* **139**: 735–748.
- 804 Chapman, N. H. and E. A. Thompson, 2002 The effect of population history on the lengths of  
805 ancestral chromosome segments. *Genetics* **162**: 449–458.
- 806 Chikhi, L., V. C. Sousa, P. Luisi, B. Goossens, and M. A. Beaumont, 2010 The confounding  
807 effects of population structure, genetic diversity and the sampling scheme on the detection  
808 and quantification of population size changes. *Genetics* **186**: 983–995.

- 809 Eguiarte, L. E., A. Búrquez, J. Rodríguez, M. Martínez-Ramos, J. Sarukhán, *et al.*, 1993 Direct  
810 and indirect estimates of neighborhood and effective population size in a tropical palm,  
811 *astrocaryum mexicanum*. *Evolution* **47**: 75–87.
- 812 Epperson, B., 2003 *Geographical Genetics*. Monographs in Population Biology, Princeton Uni-  
813 versity Press.
- 814 Felsenstein, J., 1975 A pain in the torus: Some difficulties with models of isolation by distance.  
815 *The American Naturalist* **109**: 359–368.
- 816 Fox, J. and S. Weisberg, 2011 *An R Companion to Applied Regression*. Sage, Thousand Oaks CA,  
817 second edition.
- 818 Garud, N. R., P. W. Messer, E. O. Buzbas, and D. A. Petrov, 2015 Recent selective sweeps in  
819 north american *drosophila melanogaster* show signatures of soft sweeps. *PLOS Genetics* **11**:  
820 1–32.
- 821 Griffiths, R., S. Tavaré, *et al.*, 1999 The ages of mutations in gene trees. *The Annals of Applied  
822 Probability* **9**: 567–590.
- 823 Haller, B. C., J. Galloway, J. Kelleher, P. W. Messer, and P. L. Ralph, 2019 Tree-sequence  
824 recording in SLiM opens new horizons for forward-time simulation of whole genomes.  
825 *Molecular Ecology Resources* **19**: 552–566.
- 826 Haller, B. C. and P. W. Messer, 2019 Slim 3: Forward genetic simulations beyond the wright–  
827 fisher model. *Molecular biology and evolution* **36**: 632–637.
- 828 Harris, K. and R. Nielsen, 2013 Inferring demographic history from a spectrum of shared  
829 haplotype lengths. *PLOS Genetics* **9**: 1–20.
- 830 Huillet, T. and M. Möhle, 2011 On the extended Moran model and its relation to coalescents  
831 with multiple collisions. *Theoretical Population Biology* pp. –.
- 832 Jay, F., P. Sjödin, M. Jakobsson, and M. G. Blum, 2012 Anisotropic Isolation by Distance: The  
833 Main Orientations of Human Genetic Differentiation. *Molecular Biology and Evolution* **30**:  
834 513–525.
- 835 Kang, H. M., J. H. Sul, S. K. Service, N. A. Zaitlen, S.-y. Kong, *et al.*, 2010 Variance component  
836 model to account for sample structure in genome-wide association studies. *Nature Genetics*  
837 **42**: 348 EP –.
- 838 Kang, H. M., N. A. Zaitlen, C. M. Wade, A. Kirby, D. Heckerman, *et al.*, 2008 Efficient control  
839 of population structure in model organism association mapping. *Genetics* **178**: 1709–1723.

- 840 Kelleher, J., A. Etheridge, and N. Barton, 2014 Coalescent simulation in continuous space:  
841     Algorithms for large neighbourhood size. *Theoretical Population Biology* **95**: 13 – 23.
- 842 Kelleher, J., A. M. Etheridge, and G. McVean, 2016 Efficient coalescent simulation and ge-  
843     nealogical analysis for large sample sizes. *PLoS Comput Biol* **12**: 1–22.
- 844 Kelleher, J., K. R. Thornton, J. Ashander, and P. L. Ralph, 2018 Efficient pedigree recording for  
845     fast population genetics simulation. *PLOS Computational Biology* **14**: 1–21.
- 846 Kerster, H. W., 1964 Neighborhood size in the rusty lizard, *sceloporus olivaceus*. *Evolution* **18**:  
847     445–457.
- 848 Khera, A. V., M. Chaffin, K. G. Aragam, M. E. Haas, C. Roselli, *et al.*, 2018 Genome-wide poly-  
849     genic scores for common diseases identify individuals with risk equivalent to monogenic  
850     mutations. *Nature Genetics* **50**: 1219–1224.
- 851 Kingman, J., 1982 The coalescent. *Stochastic Processes and their Applications* **13**: 235 – 248.
- 852 Lawson, D. J., N. M. Davies, S. Haworth, B. Ashraf, L. Howe, *et al.*, 2019 Is population structure  
853     in the genetic biobank era irrelevant, a challenge, or an opportunity? *Human Genetics* .
- 854 Liu, X. and Y.-X. Fu, 2015 Exploring population size changes using snp frequency spectra.  
855     *Nature Genetics* **47**: 555 EP –.
- 856 Lundgren, E. and P. L. Ralph, 2018 Are populations like a circuit? The relationship between  
857     isolation by distance and isolation by resistance. *bioRxiv* .
- 858 Martin, A. R., M. Kanai, Y. Kamatani, Y. Okada, B. M. Neale, *et al.*, 2019 Clinical use of current  
859     polygenic risk scores may exacerbate health disparities. *Nature Genetics* **51**: 584–591.
- 860 Maruyama, T., 1972 Rate of decrease of genetic variability in a two-dimensional continuous  
861     population of finite size. *Genetics* **70**: 639–651.
- 862 Mathieson, I. and G. McVean, 2012 Differential confounding of rare and common variants in  
863     spatially structured populations. *Nature Genetics* **44**: 243 EP –.
- 864 Mazet, O., W. Rodríguez, S. Grusea, S. Boitard, and L. Chikhi, 2015 On the importance of being  
865     structured: instantaneous coalescence rates and human evolution—lessons for ancestral  
866     population size inference? *Heredity* **116**: 362 EP –.
- 867 Miles, A. and N. Harding, 2017 *cghg/scikit-allel*: v1.1.8.
- 868 Neel, M. C., K. McKelvey, N. Ryman, M. W. Lloyd, R. Short Bull, *et al.*, 2013 Estimation of effec-  
869     tive population size in continuously distributed populations: there goes the neighborhood.  
870     *Heredity* **111**: 189 EP –.

- 871 Novembre, J. and M. Slatkin, 2009 Likelihood-based inference in isolation-by-distance models  
872 using the spatial distribution of low-frequency alleles. *Evolution* **63**: 2914–2925.
- 873 Pamilo, P., 1983 Genetic differentiation within subdivided populations of formica ants. *Evolu-*  
874 *tion* **37**: 1010–1022.
- 875 Patterson, N., A. L. Price, and D. Reich, 2006 Population structure and eigenanalysis. *PLOS*  
876 *Genetics* **2**: 1–20.
- 877 Price, A. L., N. J. Patterson, R. M. Plenge, M. E. Weinblatt, N. A. Shadick, *et al.*, 2006 Principal  
878 components analysis corrects for stratification in genome-wide association studies. *Nature*  
879 *Genetics* **38**: 904 EP –.
- 880 Pritchard, J. K., M. Stephens, and P. Donnelly, 2000 Inference of population structure using  
881 multilocus genotype data. *Genetics* **155**: 945–959.
- 882 Ptak, S. E. and M. Przeworski, 2002 Evidence for population growth in humans is confounded  
883 by fine-scale population structure. *Trends in Genetics* **18**: 559–563.
- 884 Purcell, S., B. Neale, K. Todd-Brown, L. Thomas, M. A. Ferreira, *et al.*, 2007 Plink: A tool set for  
885 whole-genome association and population-based linkage analyses. *The American Journal*  
886 *of Human Genetics* **81**: 559 – 575.
- 887 R Core Team, 2018 *R: A Language and Environment for Statistical Computing*. R Foundation for  
888 Statistical Computing, Vienna, Austria.
- 889 Ralph, P. and G. Coop, 2013 The geography of recent genetic ancestry across Europe. *PLoS*  
890 *Biol* **11**: e1001555.
- 891 Ringbauer, H., G. Coop, and N. H. Barton, 2017 Inferring recent demography from isolation  
892 by distance of long shared sequence blocks. *Genetics* **205**: 1335–1351.
- 893 Robledo-Arnuncio, J. J. and F. Rousset, 2010 Isolation by distance in a continuous population  
894 under stochastic demographic fluctuations. *Journal of Evolutionary Biology* **23**: 53–71.
- 895 Rousset, F., 1997 Genetic differentiation and estimation of gene flow from F-statistics under  
896 isolation by distance. *Genetics* **145**: 1219–1228.
- 897 Rousset, F. and R. Leblois, 2011 Likelihood-based inferences under isolation by distance:  
898 Two-dimensional habitats and confidence intervals. *Molecular Biology and Evolution* **29**:  
899 957–973.
- 900 Sawyer, S., 1977 On the past history of an allele now known to have frequency p. *Journal of*  
901 *Applied Probability* **14**: 439–450.

- 902 Schiffels, S. and R. Durbin, 2014 Inferring human population size and separation history from  
903 multiple genome sequences. *Nature Genetics* **46**: 919 EP –.
- 904 Schrider, D. R. and A. D. Kern, 2018 Supervised machine learning for population genetics: A  
905 new paradigm. *Trends in Genetics* **34**: 301 – 312.
- 906 Sharbel, T. F., B. Haubold, and T. Mitchell-Olds, 2000 Genetic isolation by distance in ara-  
907 bidopsis thaliana: biogeography and postglacial colonization of europe. *Molecular Ecology*  
908 **9**: 2109–2118.
- 909 Sheehan, S., K. Harris, and Y. S. Song, 2013 Estimating variable effective population sizes from  
910 multiple genomes: A sequentially markov conditional sampling distribution approach.  
911 *Genetics* **194**: 647–662.
- 912 Shirk, A. J. and S. A. Cushman, 2014 Spatially-explicit estimation of wright's neighborhood  
913 size in continuous populations. *Frontiers in Ecology and Evolution* **2**: 62.
- 914 Sohail, M., R. M. Maier, A. Ganna, A. Bloemendal, A. R. Martin, *et al.*, 2018 Signals of polygenic  
915 adaptation on height have been overestimated due to uncorrected population structure in  
916 genome-wide association studies. *bioRxiv* .
- 917 St. Onge, K. R., A. E. Palmé, S. I. Wright, and M. Lascoux, 2012 Impact of sampling schemes on  
918 demographic inference: An empirical study in two species with different mating systems  
919 and demographic histories. *G3: Genes, Genomes, Genetics* **2**: 803–814.
- 920 Städler, T., B. Haubold, C. Merino, W. Stephan, and P. Pfaffelhuber, 2009 The impact of sam-  
921 pling schemes on the site frequency spectrum in nonequilibrium subdivided populations.  
922 *Genetics* **182**: 205–216.
- 923 Tajima, F., 1989 Statistical method for testing the neutral mutation hypothesis by DNA poly-  
924 morphism. *Genetics* **123**: 585–595.
- 925 Terhorst, J., J. A. Kamm, and Y. S. Song, 2016 Robust and scalable inference of population  
926 history from hundreds of unphased whole genomes. *Nature Genetics* **49**: 303 EP –.
- 927 Wahlund, S., 1928 Zusammensetzung von populationen und korrelationserscheinungen vom  
928 standpunkt der vererbungslehre aus betrachtet. *Hereditas* **11**: 65–106.
- 929 Wakeley, J., 1999 Nonequilibrium migration in human history. *Genetics* **153**: 1863–1871.
- 930 Wakeley, J., 2005 *Coalescent Theory, an Introduction*. Roberts and Company, Greenwood Village,  
931 CO.
- 932 Wakeley, J. and T. Takahashi, 2003 Gene genealogies when the sample size exceeds the effective

- 933 size of the population. *Mol Biol Evol* **20**: 208–213.
- 934 Wickham, H., 2016 *ggplot2: Elegant Graphics for Data Analysis*. Springer-Verlag New York.
- 935 Wilke, C. O., 2019 *cowplot: Streamlined Plot Theme and Plot Annotations for 'ggplot2'*. R package  
936 version 0.9.4.
- 937 Wilkins, J. F., 2004 A separation-of-timescales approach to the coalescent in a continuous  
938 population. *Genetics* **168**: 2227–2244.
- 939 Wright, S., 1931 Evolution in mendelian populations. *Genetics* **16**: 97.
- 940 Wright, S., 1943 Isolation by distance. *Genetics* **28**: 114–138.
- 941 Wright, S., 1946 Isolation by distance under diverse systems of mating. *Genetics* **31**: 336.
- 942 Young, A. I., M. L. Frigge, D. F. Gudbjartsson, G. Thorleifsson, G. Bjornsdottir, *et al.*, 2018  
943 Relatedness disequilibrium regression estimates heritability without environmental bias.  
944 *Nature Genetics* **50**: 1304–1310.
- 945 Young, H. J., 1988 Neighborhood size in a beetle pollinated tropical aroid: effects of low  
946 density and asynchronous flowering. *Oecologia* **76**: 461–466.
- 947 Yu, J., G. Pressoir, W. H. Briggs, I. Vroh Bi, M. Yamasaki, *et al.*, 2005 A unified mixed-model  
948 method for association mapping that accounts for multiple levels of relatedness. *Nature  
949 Genetics* **38**: 203 EP –.
- 950 Zähle, I., J. T. Cox, and R. Durrett, 2005 The stepping stone model. II. Genealogies and the  
951 infinite sites model. *Ann. Appl. Probab.* **15**: 671–699.

952 **Supplementary Figures and Tables**

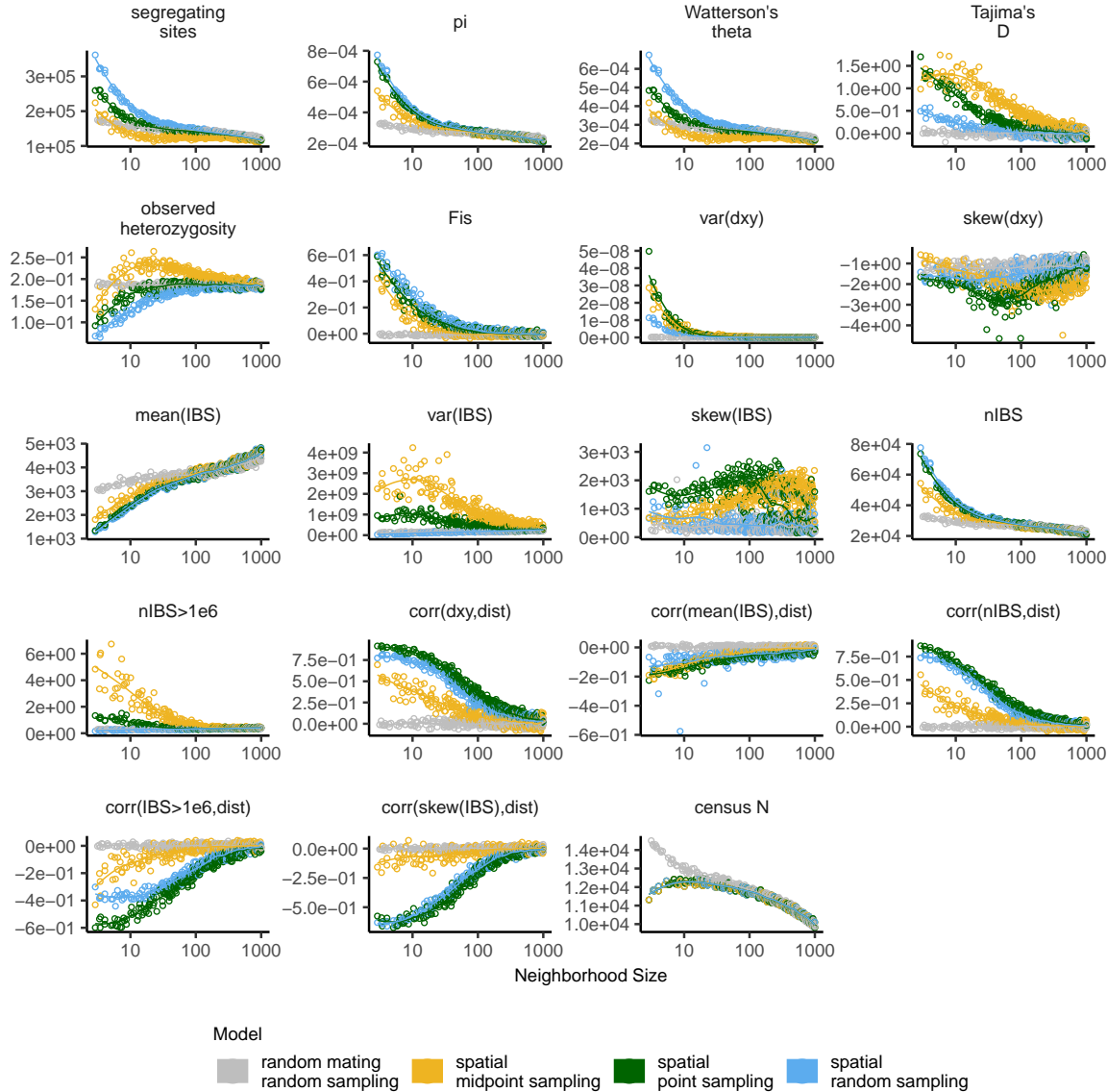


**Figure S1** Change in summary statistics by neighborhood size and sampling scheme calculated from simulated sequence data of 60 individuals.

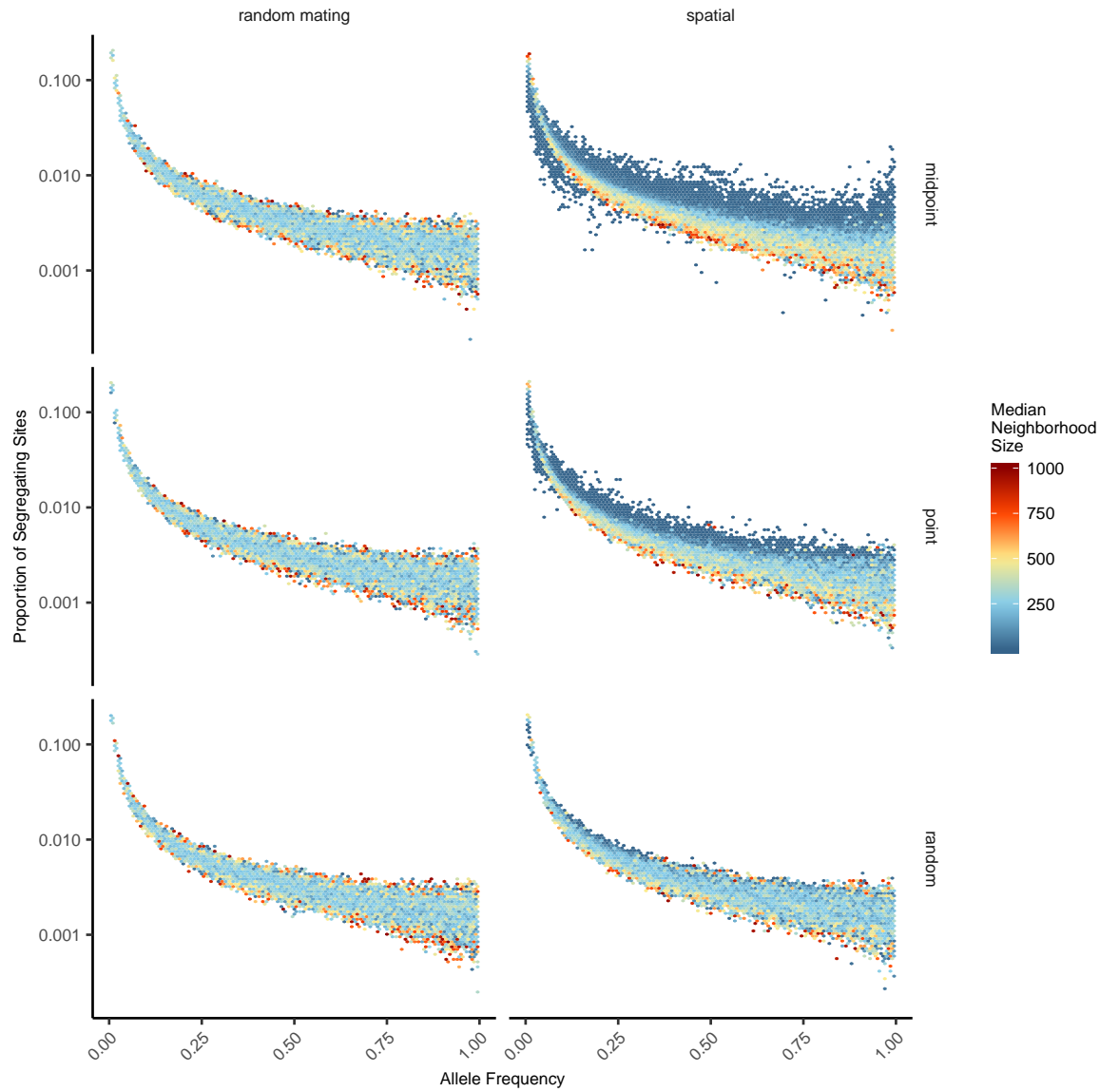


**Figure S2** Site frequency spectra for random mating and spatial SLiM models under all sampling schemes.

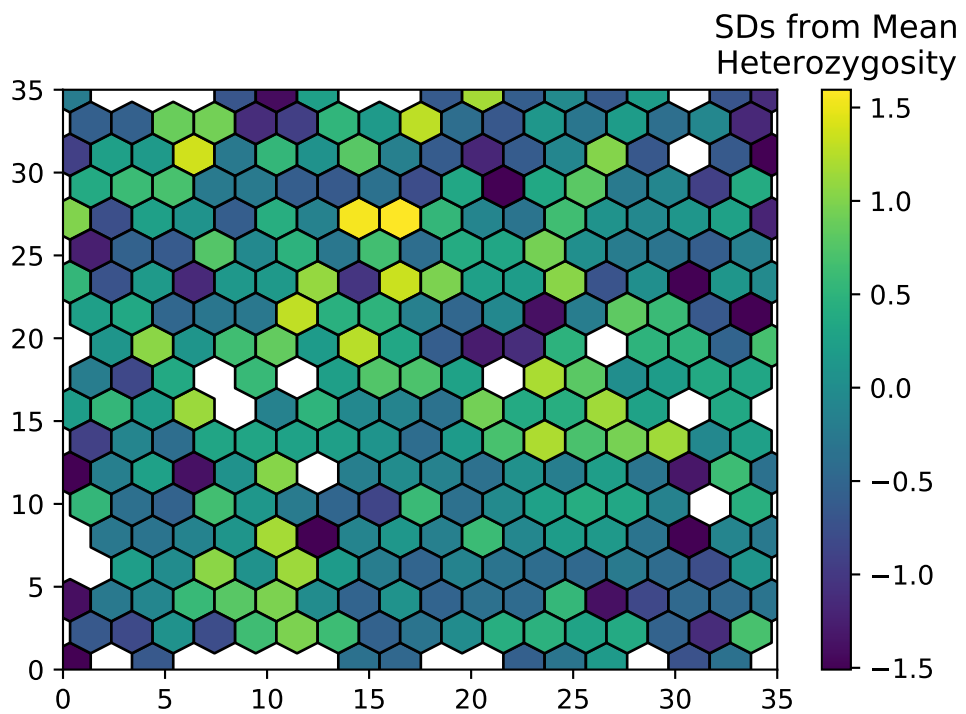
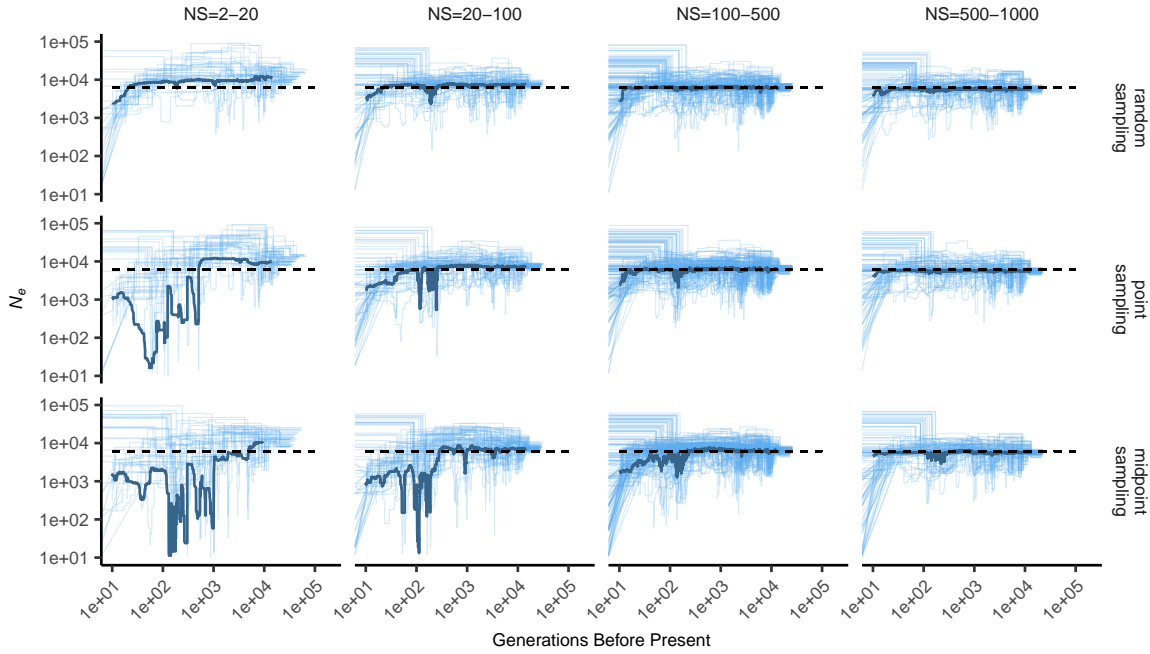


**Figure S3** Normalized mean observed heterozygosity by location across 200 randomly-sampled individuals

Stairwayplot



SMC++

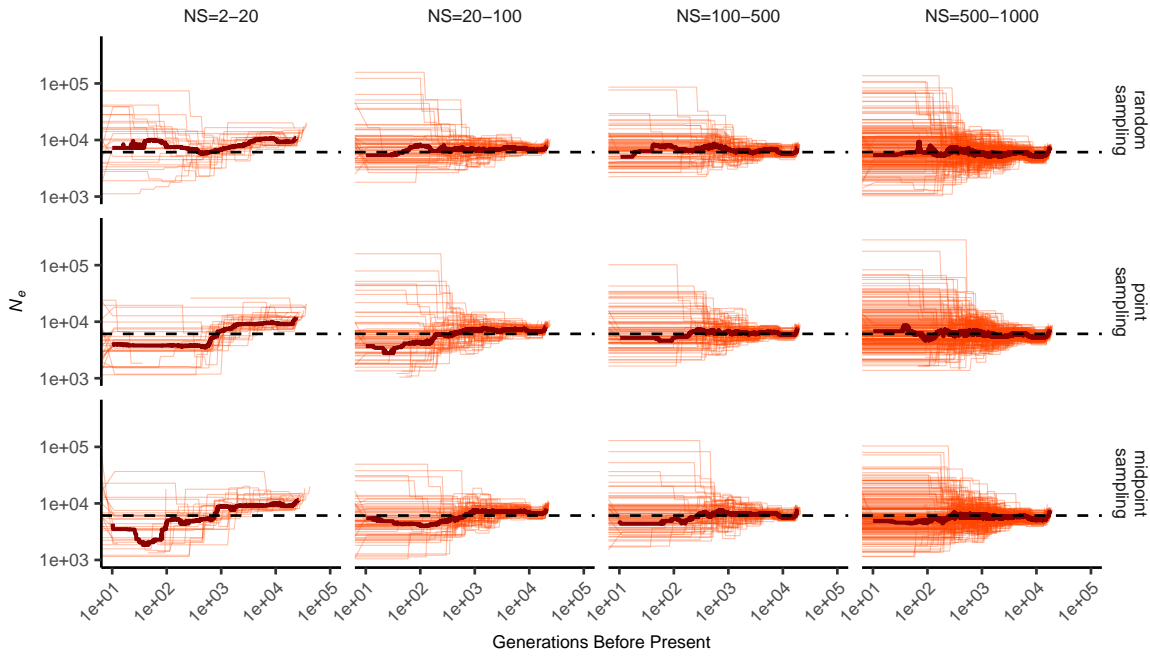


**Figure S4** Inferred demographic histories for spatial SLiM simulations, by sampling scheme and neighborhood size (NS) range. Thick lines are rolling medians across all simulations in a bin and thin lines are best fit models for each simulation. Dashed horizontal lines are the average  $N_e$  across random-mating SLiM models estimated from  $\theta_\pi$ .

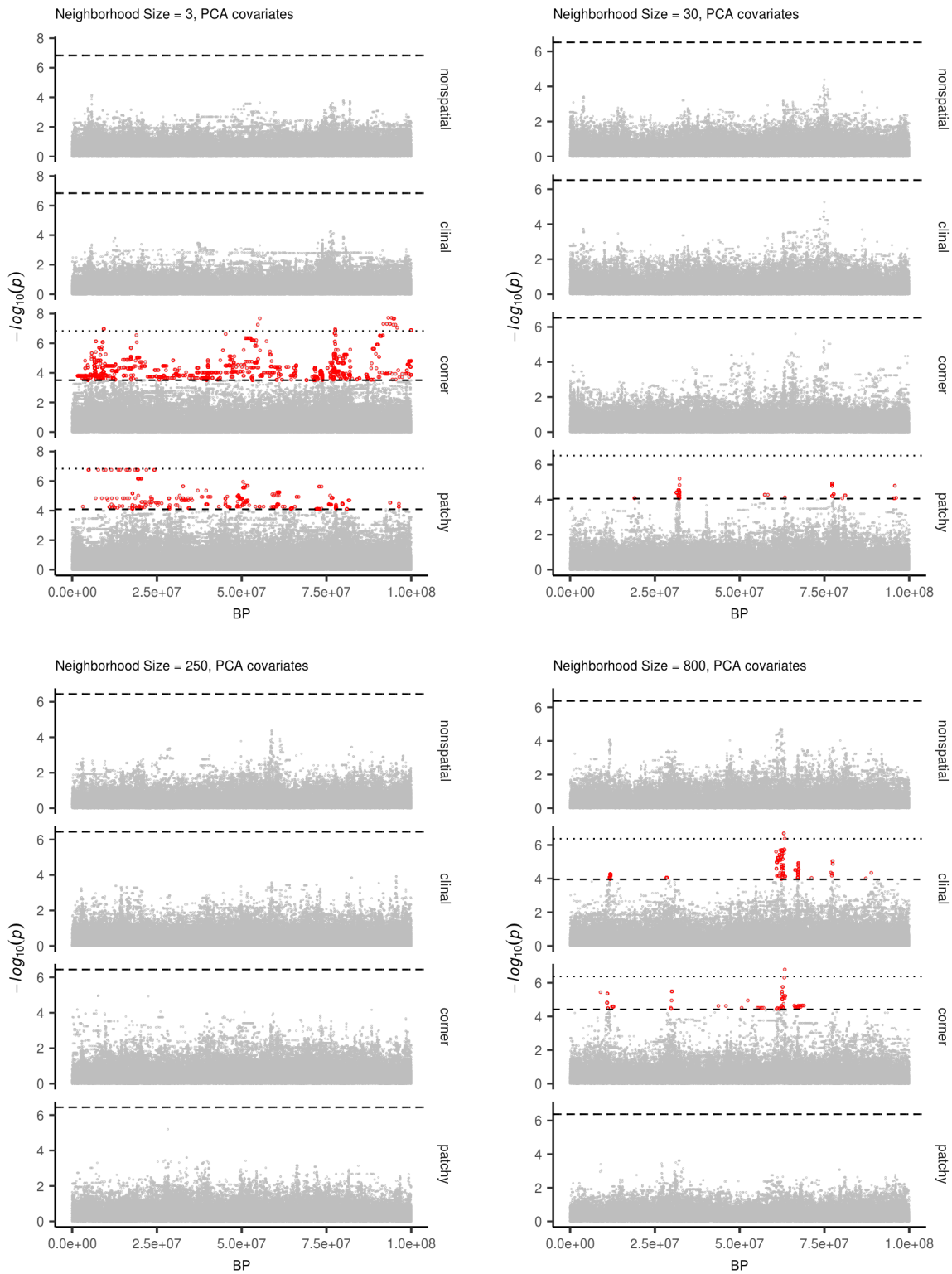


**Figure S5** Manhattan plots for a sample of simulations at varying neighborhood sizes. Labels on the right of each plot describes the spatial distribution of environmental factors (described in the methods section of the main text). Points in red are significantly associated with a nongenetic phenotype using a 5% FDR threshold (dashed line). For runs with significant associations the dotted line is a Bonferroni-adjusted threshold. Effects of common variants in space 43

**Table S1** Summary statistics calculated on simulated genotypes.

Statistic	Description
$\Theta_{pi}$	Mean of the distribution of pairwise genetic differences
$\Theta_W$	Effective population size based on segregating sites
Segregating Sites	Total number of segregating sites in the sample
Tajima's $D$	Difference in $\Theta_{pi}$ and $\Theta_W$ over its standard deviation
Observed Heterozygosity	Proportion of heterozygous individuals in the sample
$F_{IS}$	Wright's inbreeding coefficient $1 - H_e / H_o$
$var(D_{xy})$	Variance in the distribution of pairwise genetic distances
$skew(D_{xy})$	Skew of the distribution of pairwise genetic distances
$mean(IBS)$	Mean of the distribution of pairwise identical-by-state (IBS) tract lengths taken over all pairs.
$var(IBS)$	Variance of the distribution of pairwise identical-by-state (IBS) tract lengths taken over all pairs.
$skew(IBS)$	Skew of the distribution of pairwise identical-by-state (IBS) tract lengths taken over all pairs.
$nIBS$	Mean number of IBS tracts with length > 2bp across all pairs in the sample.
$nIBS > 1e6$	Mean number of IBS tracts over $1 \times 10^6$ bp per pair across all pairs in the sample.
$corr(D_{xy}, dist)$	Pearson correlation between genetic distance and $\log_{10}(spatial\ distance)$
$corr(mean(IBS), dist)$	Pearson correlation between the mean of the IBS tract distribution for each pair of samples and $\log_{10}(spatial\ distance)$
$corr(nIBS, dist)$	Pearson correlation between the number of IBS tracts for each pair of samples and $\log_{10}(spatial\ distance)$
$corr(IBS > 1e6, dist)$	Pearson correlation between the number of IBS tracts > $1 \times 10^6$ bp for each pair of samples and $\log_{10}(spatial\ distance)$
$corr(skew(IBS), dist)$	Pearson correlation between the skew of the distribution of pairwise haplotype block lengths for each pair of samples and $\log_{10}(spatial\ distance)$

**Table S2 Anova and Levene's test  $p$  values for differences by sampling strategy. Bolded values are rejected at  $\alpha = 0.05$**

variable	model	$p(\text{equal means})$	$p(\text{equal variance})$
segsites	random mating	0.998190	0.980730
$\Theta_\pi$	random mating	0.997750	0.996450
$\Theta_W$	random mating	0.998190	0.980730
Tajima's $D$	random mating	0.879690	0.188770
observed heterozygosity	random mating	0.531540	0.433230
$F_{is}$	random mating	0.474790	0.785730
$\text{mean}(D_{xy})$	random mating	0.997770	0.996510
$\text{var}(D_{xy})$	random mating	0.283630	0.647240
$\text{skew}(D_{xy})$	random mating	0.958320	0.260750
$\text{corr}(D_{xy}, \text{dist})$	random mating	0.601980	<b>0.000000</b>
$\text{mean}(IBS)$	random mating	0.997960	0.997730
$\text{var}(IBS)$	random mating	0.486450	0.399490
$\text{skew}(IBS)$	random mating	0.117980	0.069770
$nIBS$	random mating	0.997680	0.996570
$nIBS > 1e6$	random mating	0.834870	0.888730
$\text{corr}(\text{mean}(IBS), \text{dist})$	random mating	0.073270	0.308420
$\text{corr}(IBS > 1e6, \text{dist})$	random mating	0.268440	<b>0.002100</b>
$\text{corr}(\text{skew}(IBS), \text{dist})$	random mating	0.396920	<b>0.000620</b>
$\text{corr}(nIBS, \text{dist})$	random mating	0.581090	<b>0.000000</b>
segsites	spatial	<b>0.000000</b>	<b>0.000000</b>
$\Theta_\pi$	spatial	<b>0.026510</b>	0.013440
$\Theta_W$	spatial	<b>0.000000</b>	<b>0.000000</b>
Tajima's $D$	spatial	<b>0.000000</b>	<b>0.000000</b>
observed heterozygosity	spatial	<b>0.000000</b>	<b>0.000000</b>
$F_{is}$	spatial	<b>0.000000</b>	0.000120
$\text{mean}(D_{xy})$	spatial	<b>0.025390</b>	0.012910
$\text{var}(D_{xy})$	spatial	<b>0.004970</b>	0.006230
$\text{skew}(D_{xy})$	spatial	<b>0.000000</b>	<b>0.000000</b>
$\text{corr}(D_{xy}, \text{dist})$	spatial	<b>0.000000</b>	<b>0.000000</b>
$\text{mean}(IBS)$	spatial	0.272400	0.114250
$\text{var}(IBS)$	spatial	<b>0.000000</b>	<b>0.000000</b>
$\text{skew}(IBS)$	spatial	<b>0.000000</b>	<b>0.000000</b>
$nIBS$	spatial	<b>0.033920</b>	0.016640
$nIBS > 1e6$	spatial	<b>0.000000</b>	<b>0.000000</b>
$\text{corr}(\text{mean}(IBS), \text{dist})$	spatial	<b>0.000000</b>	0.590540
$\text{corr}(IBS > 1e6, \text{dist})$	spatial	<b>0.000000</b>	<b>0.000000</b>
$\text{corr}(\text{skew}(IBS), \text{dist})$	spatial	<b>0.000000</b>	<b>0.000000</b>
$\text{corr}(nIBS, \text{dist})$	spatial	<b>0.000000</b>	<b>0.000000</b>